Review

Generalised Parton Distributions in Continuum Schwinger Methods: Progresses, Opportunities and Challenges

Cédric Mezrag

Review

Generalised Parton Distributions in Continuum Schwinger Methods: Progresses, Opportunities and Challenges

Cédric Mezrag

Institut de Recherche sur les lois Fondamentales de L'univers, Commissariat à L'énergie Atomique et aux Énergies Alternatives, Université Paris-Saclay, F-91191 Gif-sur-Yvette, France; cedric.mezrag@cea.fr

Abstract: This paper review the modelling efforts regarding Generalised Parton Distributions (GPDs) using continuum techniques relying on Dyson–Schwinger and Bethe–Salpeter equations. The definition and main properties of the GPDs are first recalled. Then, we detail the strategies developed in the last decade in the meson sector, highlighting that observables connected to the pion GPDs may be measured at future colliders. We also highlight the challenges one will face when targeting baryons in the future.

Keywords: generalised partons distributions; continuum Schwinger methods; lightfront wave functions

1. Introduction

Since the early days of QCD and the major result of Bjorken scaling [1] followed by scaling violations [2–4], hadron structure has been one of the main topics of study regarding the strong interaction. In the 1990s, the family of matrix elements connected to the structure of hadron went from uni-dimensional, Parton Distribution Functions (PDFs) and Electromagnetic Form Factors (EFF), to multi-dimensional with the introduction of Generalised Parton Distributions (GPDs) [5–7] and Transverse Momentum Dependent PDFs (TMDs) [8,9]. The former are connected to the 2D+1D picture of the nucleon [10,11] while the TMDs provide a 3D picture of momentum space. Both are defined from a matrix element of the type

$$\langle p_{\text{out}}|O\left(\frac{-z}{2},\frac{z}{2}\right)|p_{\text{in}}\rangle,\tag{1}$$

where, in the case of GPDs, the distance z is lightlike ($z^2 = 0$) and the momentum transfer $\Delta = p_{out} - p_{in}$ is finite. For TMDs, the distance z is off the lightcone ($z^2 \neq 0$) but no momentum transfer is allowed ($\Delta = 0$). They both generalise PDFs for which $z^2 = 0$ and $\Delta = 0$. Similarly, TMDs and GPDs were latter unified as two distinct limits of Generalised Transverse Momentum Dependent PDFs (GTMDs), for which both $z^2 \neq 0$ and $\Delta \neq 0$ [12–17]. GTMDs are thought to provide a 5D picture of hadrons as illustrated in Figure 1.

A wealth of theoretical studies has been dedicated in the last decade to GPDs, TMDs and GTMDs. Since it remains unclear whether some processes could be sensitive to GTMDs (despite some pioneering studies [18]), TMDs and GPDs stand at the core of experimental studies of current and future facilities. The 12 GeV upgrade of the electron beam of the Jefferson Laboratory facility (JLab 12) has been completed. JLab 12 is thus expected to deliver a wealth of very precise data that can be connected to GPDs and TMDs in the forthcoming years (and in fact data release has already started, see, e.g., [19,20]), mostly in the so-called valence region. In the next decade, the experimental community is expected to move from fixed target to collider experiments, with the planned electron-ion colliders both in the US (EIC) and China (EicC).
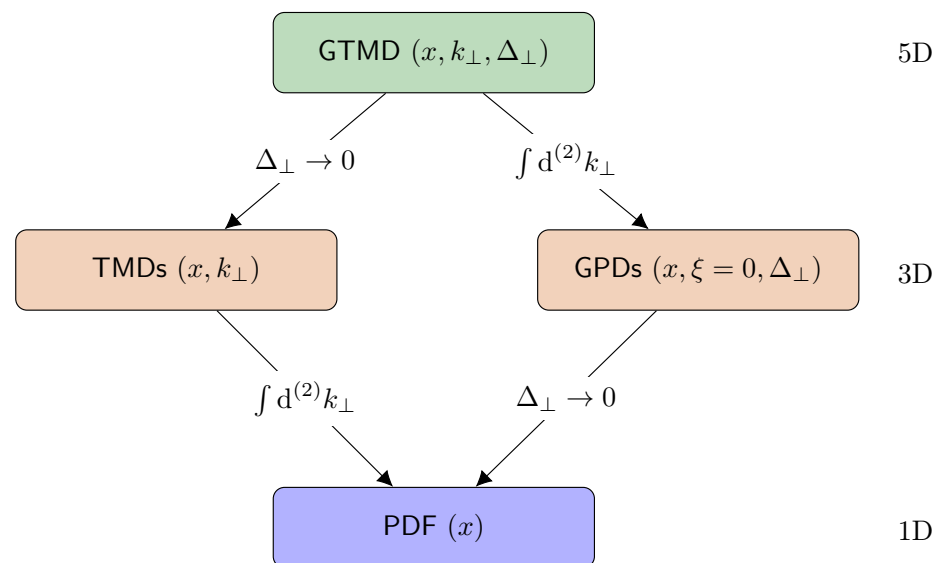
Figure 1. Family of distributions encoding hadron structure, where x is the momentum fraction along the lightcone carried by the active parton, $k_\perp$ its transverse momentum (the Fourier conjugate of $z_\perp$). $\Delta_\perp$ is the transverse momentum transferred between the initial and final hadron state. At this stage, the integrals over $k_\perp$ should be understood as formal only, and need to be regularised, both from TMDs to PDFs [8,21,22] and from GTMDs to GPDs [23]. This picture is valid for vanishing skewness ξ, i.e., no momentum transfer along the lightcone is allowed.

In parallel with experimental facilities, ab initio computational methods have made major progress in the last decade. Lattice-QCD is now able to compute data related directly to the x-dependence of distributions [24–26] instead of solely the first few Mellin moments. This breakthrough has triggered many computing efforts, attempting to perform computations of Distribution Amplitudes (DA), PDFs and GPDs (see, e.g., [27–29]). These steps are very promising but many more remain to be taken before precision studies can be performed on the lattice.

In parallel, non-perturbative studies using continuum techniques such as Bethe–Salpeter equations have also been developed in the past decade, targeting the x-dependence of hadron structure, after the computations of local operators (mostly the EFFs). The main developments came from the use of spectral representations (or Nakanishi representations [30,31]) and analysis of the singularities in the complex plane (see the recent example [32,33]). The breakthrough in the computation of QCD three-point functions [34–36] is also very promising in terms of the ability to reach realistic computations of hadron structure and there interpretation (see, for instance, the case of the gluon mass generation through the Schwinger mechanism [37]). Indeed, continuum techniques based on Dyson–Schwinger and Bethe–Salpeter equations offer a unique window to understand the emergent phenomena in QCD through their ability to select subsets of QCD effects in systematic ways which carefully guarantee that underlying QCD symmetries remain fulfilled.

In this review article, we will focus on GPDs. The latter have already been the main topic of several theoretically oriented [38,39] and phenomenologically oriented [40] review papers and lectures (see, for instance, [41]). Here, we will highlight the efforts in the last decade regarding their computations using continuum formalisms, and thus partly updating them [42]. In Section 2, we will remind the readers the formal definition of GPDs, the properties they should obey from QCD, and explain why phenomenological extractions are challenging. In Section 3, we will discuss the efforts which have been undertaken to compute these GPDs in the meson sector, highlighting the successes and challenges. Then, in Section 4, we will review the pioneering work in the baryon sector, and highlight the future possibilities offered by the continuum formalism.

2. Generalised Parton Distributions

2.1. Formal Definitions and First Properties

Introduced in the 1990s in three distinct series of papers [5–7,43,44], GPDs can be formally defined as off-diagonal matrix elements of a non-local operator in momentum space. The operator is evaluated at light-like distances such that, in the case of the pion, GPDs are defined as:

$$H_\pi^q(x,\xi,t) = \frac{1}{2}\int\frac{\mathrm{d}z^-}{2\pi}e^{ixP^+z^-}\langle p_2|\bar{\psi}^q\left(-\frac{z^-}{2}\right)\mathcal{W}\left(-\frac{z^-}{2},\frac{z^-}{2}\right)\gamma^+\psi^q\left(\frac{z^-}{2}\right)|p_1\rangle, \quad (2)$$

$$H_\pi^g(x,\xi,t) = \frac{1}{P^+}\int\frac{\mathrm{d}z^-}{2\pi}e^{ixP^+z^-}\langle p_2|G^{+\mu}\left(-\frac{z^-}{2}\right)\mathcal{W}\left(-\frac{z^-}{2},\frac{z^-}{2}\right)G_\mu^+\left(\frac{z^-}{2}\right)|p_1\rangle, \quad (3)$$

where ψ^q is a quark field of flavour q and $G^{\mu\nu}$ is the gluon field strength. The + component indicates the lightcone direction following the standard conventions of:

$$z^\pm = \frac{1}{\sqrt{2}}(z^0 \pm z^3), \quad z^\perp = (z^1,z^2), \quad (4)$$

$$z^2 = 2z^+z^- - z_\perp^2. \quad (5)$$

The average momentum of the hadron P and the momentum transfer Δ are conveniently defined as:

$$P = \frac{p_1 + p_2}{2}, \quad \Delta = p_2 - p_1. \quad (6)$$

This allows us to simply express the variables (ξ,t) whose definition is not manifest in Equations (2) and (3) through:

$$\xi = -\frac{\Delta^+}{2P^+}, \quad t = \Delta^2. \quad (7)$$

The definition domain of GPDs in x and ξ is illustrated in Figure 2. Finally, let us mention that $\mathcal{W}$ is the Wilson line defined as:

$$\mathcal{W}\left(-\frac{z^-}{2},\frac{z^-}{2}\right) = P\exp\left[ig\int_{-\frac{z^-}{2}}^{\frac{z^-}{2}}\mathrm{d}\zeta^- A^+(\zeta^-)\right] \quad (8)$$

where P is the path ordering between $-z^-/2$ and $z^-/2$ and g is the QCD coupling.

Because of its richer spin structure, more GPDs are necessary in order to parametrise the off-forward matrix element of the nucleon:

$$\frac{1}{2}\int\frac{\mathrm{d}z^-}{2\pi}e^{ixP^+z^-}\langle p_2|\bar{\psi}^q\left(-\frac{z^-}{2}\right)\gamma^+\mathcal{W}\left(-\frac{z^-}{2},\frac{z^-}{2}\right)\psi^q\left(\frac{z^-}{2}\right)|p_1\rangle$$
$$=\frac{1}{2P^+}\left(H^q(x,\xi,t)\bar{u}(p_2)\gamma^+u(p_1) + E^q(x,\xi,t)u(p_2)\frac{i\sigma^{+\nu}\Delta_\nu}{2M}u(p_1)\right), \quad (9)$$

for quarks and

$$\frac{1}{P^+}\int\frac{\mathrm{d}z^-}{2\pi}e^{ixP^+z^-}\langle p_2|G^{+\mu}\left(-\frac{z^-}{2}\right)\mathcal{W}\left(-\frac{z^-}{2},\frac{z^-}{2}\right)G_\mu^+\left(\frac{z^-}{2}\right)|p_1\rangle$$
$$=\frac{1}{2P^+}\left(H^g(x,\xi,t)\bar{u}(p_2)\gamma^+u(p_1) + E^g(x,\xi,t)u(p_2)\frac{i\sigma^{+\nu}\Delta_\nu}{2M}u(p_1)\right), \quad (10)$$

for gluons. Quark and gluon polarised distributions can also be defined for the nucleon (see, e.g., [38]). However, since we do not use them in the following, we do not introduce them here. Similarly, transversity GPDs are not introduced in this review paper.
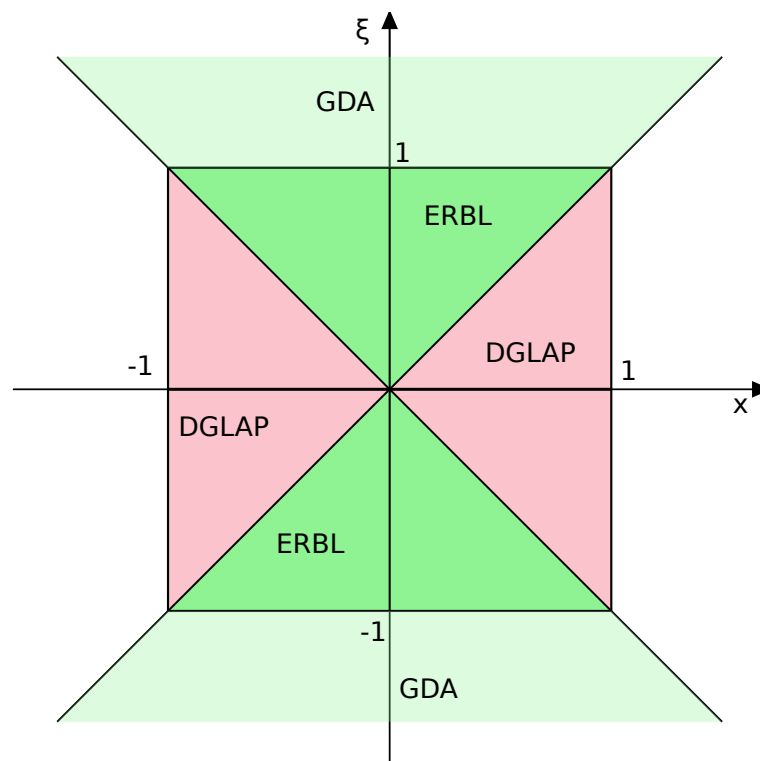
Figure 2. The GPD definition domain in x and ξ. The so-called DGLAP (or outer) region for which $|x| \geq |\xi|$ is shaded in pink, while the ERBL (or inner) region for which $|x| \leq |\xi|$ is shaded in green. The ERBL region can be extended for $|\xi| \geq 1$ (lighter green) where GPDs can be related to Generalised Distribution Amplitude [45–48] through analytic continuations thanks to the crossing symmetry.

The off-forward nature of GPDs triggers interesting consequences, as the incoming and outgoing partons carry a momentum fraction expressed as $x \pm \xi$. Several cases can be drawn, as illustrated in Figure 2. The complete GPD support draws a square such that $(x, \xi) \in [-1, 1]^2$ (see ref. [49] for the derivation of the GPD definition domain). Within this domain, two types of regions can be highlighted: the outer one for which $|x| \geq |\xi|$, and the inner one where $|\xi| \geq |x|$. The former is called the DGLAP region (Dokshitzer, Gribov, Lipatov, Altarelli, Parisi) while the latter is labelled the ERBL region (Efremov–Radyushkin–Brodsky–Lepage). This distinction comes from the fact that the two regions present different physical interpretations when considering probed partons. Indeed, the incoming and outgoing partons momentum fraction can be expressed as $x \pm \xi$. Thus, in the quark sector, depending of the sign of this combination, one probes a quark or an antiquark. Figure 3 illustrates the different possibilities highlighting the specificity of the inner region with respect to the outer ones. There, the interpretation yields an exchange of a pair of quark and anti-quark in the t channel. On the other hand, the outer region can be seen as probing an active quark by taking it out and putting it back within the nucleon. These different interpretations have a major impact as the evolution equations will significantly vary between the two regions, hence the two names from famous evolution equations, DGLAP [2–4] and ERBL [50–53].

The discussion of evolution properties leads us to mention the symmetry of GPDs regarding the lightcone momentum fractions. Pion and nucleon GPDs present interesting symmetry properties: they are even in ξ because of time reversal invariance (see, e.g., [39] for a proof and list of exceptions for higher spin hadrons). In addition, gluon GPDs are

even in x within our definition, while quark GPDs have no specific x-parity. Nevertheless, x-even and x-odd combinations are often introduced as:

$$H_q^- = H^q(x, \xi, t) + H^q(-x, \xi, t), \tag{11}$$

$$H_q^+ = H^q(x, \xi, t) - H^q(-x, \xi, t), \tag{12}$$

where $+$ and $-$, respectively, mean singlet and non-singlet combinations. Note that in case of multiple quark flavour, the real singlet component has to be summed over the flavours. These combinations are often introduced as the singlet combination mixes with gluons under evolution, while the non-singlet one does not.
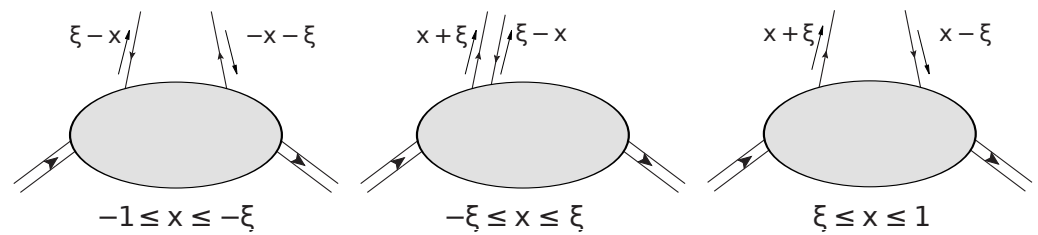

Figure 3. The DGLAP or ERBL regions and their different interpretations in terms of partons. From left to right, one goes through the antiquark interpretation of the probed parton. Then, in the inner region $-\xi < x < \xi$, one recovers the ERBL region and its interpretation as the "extraction" of a quark–antiquark pair from the hadron. Finally, on the right-hand side, $\xi < x < 1$ and we recover the quark interpretation of the DGLAP region.

2.2. Reduction to Unidimensional Distributions

When taking the forward limit of the matrix elements defined in (2) and (3), i.e., when no momentum transfer is allowed, one recovers the standard PDFs as:

$$H^q(x, 0, 0) = q(x)\theta(x) - \bar{q}(-x)\theta(-x), \tag{13}$$

$$H^g(x, 0, 0) = xg(x)\theta(x) - xg(-x)\theta(-x), \tag{14}$$

where θ is the Heaviside function. Through the forward limit, PDFs have been a key ingredient in GPD modelling strategies since they were introduced [54–59].

GPDs are also connected with EFFs through integration over the x variable. The quark flavour q contribution to the Dirac form factor F_1 and the Pauli form factor F_2 can be obtained from GPDs as:

$$\int dx\, H^q(x, \xi, t) = F_1^q(t) \tag{15}$$

$$\int dx\, E^q(x, \xi, t) = F_2^q(t) \tag{16}$$

Until now, the EFFs sum rules presented here have been one of the main constraints applied to model the t-dependence of GPDs.

In the pion case, one can highlight an additional property. In the chiral limit, the pion quark GPD can be related to the pion distribution amplitude [46,60]:

$$H_q^-(x, 1, 0) = \varphi\left(\frac{1+x}{2}\right), \tag{17}$$

$$H_q^+(x, 1, 0) = 0. \tag{18}$$

This property is usually labelled "soft pion theorem" in the literature. As we mention above, since the singlet and gluon GPDs mix under evolution, Equation (18) implies that the gluon GPD should also vanish in the chiral limit for $(\xi, t) \to (1, 0)$.

2.3. Interpretation in Coordinate Space

GPDs are naturally defined in momentum space, as the momentum transfer Δ is the relevant experimental variable to be measured. Nevertheless, one can also define GPDs in the so-called impact parameter space (see, e.g., refs. [10,11]), by introducing the impact parameter $b_\perp$. The latter measures the distance from the centre of +-momentum within the nucleon and is connected to the momentum variable as being the Fourier conjugate of the vector D[11]:

$$D = \frac{p_2}{1-\xi} - \frac{p_1}{1+\xi}. \tag{19}$$

One can then show that a 1+2D probability density $\rho(x, b_\perp)$ can be recovered through the so-called Hankel transform of the GPDs for $\xi = 0$. In this limit, $D_\perp = \Delta_\perp$ and

$$\rho(x, 0, |b_\perp|) = \frac{1}{4\pi} \int_0^\infty d\left(\Delta_\perp^2\right) J_0(|\Delta_\perp||b_\perp|) H(x, 0, t), \tag{20}$$

where J_0 is the standard Bessel function of the first kind of order 0. Note that the impact parameter $b_\perp$ should not be confused with the Fourier conjugate of $k_\perp$ also labelled b by the TMD community.

An illustration of this probabilistic interpretation is given in Figure 4 and comes from model computations (see ref. [60] for details). In principle, it is also possible to extract these 3D distributions from experimental data (see, for instance, [61] for a recent example on the nucleon). However, three main difficulties arise:

- Collinear factorisation allows one to interpret exclusive processes in terms of GPDs for values of t much smaller than the typical hard scale of the system;
- Yet, performing the Fourier transform requires to integrate over t up to infinity, introducing model-dependent extrapolations;
- Furthermore, no experimental data is available for vanishing values of ξ, meaning that additional extrapolations generating more model biases are required.

These difficulties hardly alter the appealing possibilities offered by GPDs to map in 3D the average position of quarks and gluons within hadrons. This explains the enthusiasm in the field towards placing GPDs at the core of the physics cases of running or planned experimental facilities, such as the US [62] and Chinese [63] electron ion colliders.
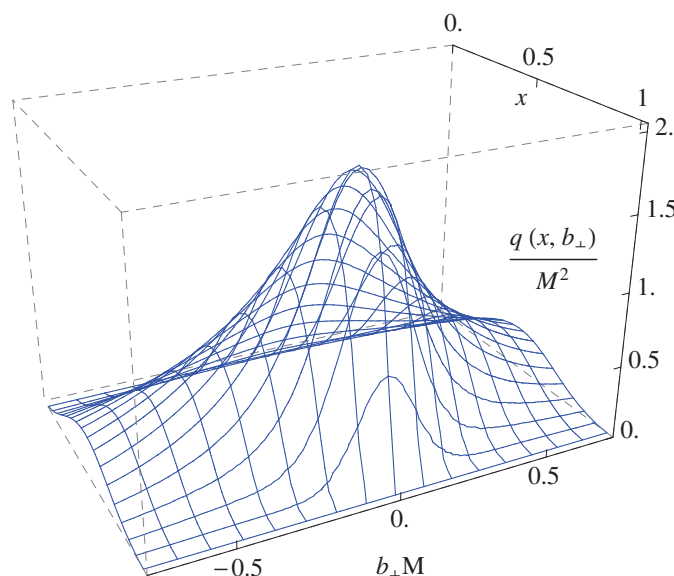

Figure 4. 3D picture of a model computation of the pion quark GPD in the impact parameter space. Figure from [60].

2.4. Connection with the Energy-Momentum Tensor

The ability to perform the 1+2D tomography of the nucleon is not the only exciting feature of GPDs. Indeed, they also allow a unique access to the hadrons' Energy-Momentum Tensor (EMT). Labelling the EMT operator T, one can parametrise the associated matrix element for the pion as [64]:

$$\langle p_2|T_a^{\mu\nu}|p_1\rangle = 2P^\mu P^\nu A^a(t) + \frac{1}{2}\left(\Delta^\mu\Delta^\nu - \eta^{\mu\nu}\Delta^2\right)C^a(t) + 2M^2\eta^{\mu\nu}\bar{C}^a(t). \tag{21}$$

where a is a generic label for quark flavour and gluon contributions, and M is the hadron mass. In the literature, the form factors A, C and $\bar{C}$ may be designated as gravitational form factors. Additional form factors are required for describing the nucleon EMT matrix element [65,66]:

$$\langle p_2|T_a^{\mu\nu}(0)|p_1\rangle = \bar{u}(p_2)\left\{ \frac{P^\mu P^\nu}{M} A^a(t) + \frac{\Delta^\mu\Delta^\nu - \eta^{\mu\nu}\Delta^2}{M} C^a(t) + M\eta^{\mu\nu}\bar{C}^a(t) \right.$$
$$\left. + \frac{i(P^\mu\sigma^{\nu\rho} + P^\nu\sigma^{\mu\rho})\Delta_\rho}{4M}[A^a(t) + B^a(t)] + \frac{P^{[\mu}i\sigma^{\nu]\rho}\Delta_\rho}{4M} D^a(t) \right\}u(p_1), \tag{22}$$

where we define the anti-symmetric combination $a^{[\mu}b^{\nu]} = a^\mu b^\nu - a^\nu b^\mu$. These form factors of the EMT have to obey specific constraints, originating from conservation laws [5,67–69]:

$$\sum_f A^{q_f}(0) + A^g(0) = 1 \tag{23}$$

$$\sum_f B^{q_f}(0) + B^g(0) = 0 \tag{24}$$

$$\sum_f \bar{C}^{q_f}(t) + \bar{C}^g(t) = 0 \tag{25}$$

where $\sum_f$ is the sum over the considered quark flavours. Some of the EFF can be related to GPDs through the computation of the first-order Mellin moments:

$$\int_{-1}^{1} dx\, x H^q(x,\xi,t) = A^q(t) + 4\xi^2 C^q(t), \tag{26}$$

$$\int_{-1}^{1} dx\, x E^q(x,\xi,t) = B^q(t) - 4\xi^2 C^q(t). \tag{27}$$

Consequently, two out of three EMT form factors are connected to GPDs in the pion case, while three out of five are in the nucleon one. The form factor $\bar{C}$ remains out of reach for leading twist distributions. In the nucleon case, the form factor D can be related to the nucleon axial form factor and thus to the polarised GPDs [70,71].

Within our conventions, the gluon EMT form factors are related to the gluon GPDs in a very similar way, with a modification of the power of the Mellin moment (consistently with the forward limit of our gluon GPDs):

$$\int_{-1}^{1} dx\, H^g(x,\xi,t) = A^g(t) + 4\xi^2 C^g(t), \tag{28}$$

$$\int_{-1}^{1} dx\, E^g(x,\xi,t) = B^g(t) - 4\xi^2 C^g(t). \tag{29}$$

From these connections between GPDs and the EMT, one can derive the famous Ji sum rule [5], allowing one to decompose the total angular momentum of the nucleon into contributions carried by each quark flavour J^q and gluons J^g:

$$2J^q = A^q(0) + B^q(0) = \int_{-1}^{1} dx\, x(H^q(x,\xi,0) + E^q(x,\xi,0)), \tag{30}$$

$$2J^g = A^g(0) + B^g(0) = \int_{-1}^{1} dx\, (H^g(x,\xi,0) + E^g(x,\xi,0)). \tag{31}$$

The A and B form factors are not the only ones providing an interesting interpretation. The C and $\bar{C}$ ones can be interpreted in terms of pressure and shear forces distributions within the hadrons [64,71–73]. For simplicity, we will only discuss here the quark and gluon contributions to the isotropic pressure p_q and p_g and the pressure anisotropy s_q and s_g. They depend on the form factors C and $\bar{C}$ in the Breit frame through [71]:

$$p_a(\vec{r}) = M \int \frac{d^3\vec{\Delta}}{(2\pi)^3} e^{-i\vec{r}\vec{\Delta}} \left[\frac{2t}{3M} C^i(t) - \bar{C}^i(t) \right], \tag{32}$$

$$s_a(\vec{r}) = \frac{4M}{r^2} \int \frac{d^3\vec{\Delta}}{(2\pi)^3} e^{-i\vec{r}\vec{\Delta}} \frac{t^{-1/2}}{M^2} \frac{d^2}{dt^2} \left[t^{5/2} C^i(t) \right]. \tag{33}$$

We highlight that the index a stands again for quark flavour and gluon contributions and $\vec{r}$ is a 3D spatial vector. One can readily note from Equation (33) that the pressure anisotropy is independent of $\bar{C}$ and thus can be fully extracted from GPDs. In addition, from Equation (32), one can realise that the total isotropic pressure is also independent of $\bar{C}$ thanks to Equation (25), and thus, one can in principle also extract it from GPDs. Finally, let us mention that this discussion is valid both for the pion and the nucleon.

Before concluding this section, we would like to highlight that in the case of the pion, there is an additional constraint on the EMT form factors, thanks to the soft pion theorem of Equation (18). Indeed, at vanishing t in the chiral limit, one has:

$$0 = \int_{-1}^{1} dx\, x H_S^q(x,1,0) = A^q(0) + 4C^q(0), \tag{34}$$

connecting the normalisation of C^q and A^q.

Finally, let us stress that H_S^q vanishes only if the gluon GPD also vanishes due to mixing of the two under evolution. Since the soft pion theorem is expected to be scale-independent, then Equation (34) can also be written for gluons.

2.5. Double Distribution Representation

The sum rules already encountered previously and connecting GPDs to the EFF and EMT Form Factors can in fact be generalised to higher-order Mellin moments by looking at the tensorial structure of local off-forward operators.

2.5.1. Local Operators Analysis

We define the m-th Mellin moment $\mathcal{M}_m$ of the GPD as:

$$\mathcal{M}_m(\xi,t) = \int_{-1}^{1} dx\, x^m H(x,\xi,t). \tag{35}$$

Through straightforward computations (see, e.g., [41]), one can connect these Mellin moments to local twist-two operators (we remain with the lightcone gauge and the pion case here):

$$\mathcal{M}_m(\xi,t) = \frac{1}{2(P^+)^{m+1}} \langle p_2 | \bar{\psi}^q(0) \gamma^+ \left(i \overleftrightarrow{\partial}^+ \right)^m \psi^q(0) | p_1 \rangle,$$

where we use

$$\overset{\leftrightarrow}{\partial}{}^{\mu} = \frac{1}{2}\left(\overset{\rightarrow}{\partial}{}^{\mu} - \overset{\leftarrow}{\partial}{}^{\mu}\right). \tag{36}$$

The Lorentz structure of the twist-two local operators $O^{\mu\mu_1\cdots\mu_m}$ is given as:

$$O^{\mu\mu_1\cdots\mu_m} = \bar{\psi}^q(0)\gamma^{\{\mu}i\overset{\leftrightarrow}{\partial}{}^{\mu_1}\ldots i\overset{\leftrightarrow}{\partial}{}^{\mu_m\}}\psi^q(0), \tag{37}$$

where $\{\ldots\}$ indicates that the Lorentz indices are symmetrised and traceless. The parametrisation of the associated matrix elements is thus given as:

$$\langle p_2|\bar{\psi}^q(0)\gamma^{\{\mu}i\overset{\leftrightarrow}{\partial}{}^{\mu_1}\ldots i\overset{\leftrightarrow}{\partial}{}^{\mu_m\}}\psi^q(0)|p_1\rangle$$
$$= P^{\{\mu}\sum_{i=1}^{m+1}P^{\mu_1}\ldots P^{\mu_{i-1}}\Delta^{\mu_i}\ldots\Delta^{\mu_m\}}A^q_{i,m}(t) + \Delta^{\{\mu}\Delta^{\mu_1}\ldots\Delta^{\mu_m\}}C^q_{m+1}(t), \tag{38}$$

in the pion case. $A_{i,m}$ and C_{m+1} are called generalised form factors, and only depend on t and μ^2. Moreover, due to discrete symmetries, only even powers of ξ contribute, and the Mellin moments of the pion GPD can be written as:

$$\mathcal{M}_m(\xi,t) = \sum_{i=0}^{\left[\frac{m}{2}\right]}(2\xi)^{2i}A^q_{i,m}(t) + \mathrm{mod}(m,2)(2\xi)^{m+1}C_{m+1}(t), \tag{39}$$

where $[\ldots]$ designates the floor function and $\mathrm{mod}(2,m)$ vanishes if m is even, and is 1 otherwise. Equation (39) is commonly labelled the polynomiality property of GPDs [74,75]. It generalises the sum rules between GPDs, EFFs and EMT form factors, already highlighted in Equations (15) and (26) in the case of the pion. For the nucleon, additional tensorial structures allow one to generalise Equations (15) and (27).

2.5.2. The Radon Transform and the Specific Role of the D-Term

The C_{m+1} generalised form factors play a specific role in the decomposition of the GPD matrix element. They are the moment of an x-odd generating function called the D-term (we highlight that the D-term $D(y,t)$ is connected to the EMT FF $C(t)$ and not $D(t)$; this notation discrepancy is unfortunate but standard in the contemporary literature) and defined through:

$$\int_{-1}^{1}\mathrm{d}y\,y^m D(y,t) = (2)^{m+1}C_{m+1}(t). \tag{40}$$

The proof of existence of the function D is not simple and related to the Hausdorff moment problem [76,77]. In the following, we assume that D exists and is unique. The polynomiality property becomes:

$$\sum_{i=0}^{\left[\frac{m}{2}\right]}(2\xi)^{2i}A^q_{i,m}(t) = \int_{-1}^{1}\mathrm{d}x\,x^m H(x,\xi,t) - \xi^{m+1}\int_{-1}^{1}\mathrm{d}y\,y^m D(y,t). \tag{41}$$

By rescaling the variable $y \to x/\xi$ for $\xi > 0$, one obtains:

$$\sum_{i=0}^{\left[\frac{m}{2}\right]}(2\xi)^{2i}A^q_{i,m}(t) = \int_{-1}^{1}\mathrm{d}x\,x^m\left[H(x,\xi,t) - D\left(\frac{x}{\xi},t\right)\mathbb{I}_{-\xi\leq x\leq\xi}\right], \tag{42}$$

where $\mathbb{I}_{-\xi\leq x\leq\xi}$ is 1 for $x \in [-\xi;\xi]$ and 0 otherwise. On top of telling us that the D-term is a function of the ratio x/ξ, Equation (42) highlights that the D-term has support only in the ERBL region. Moreover, the typical polynomial structure of degree n of the nth Mellin moments of $H - D$ is known in mathematics as the the Lugwig–Hegalson consistency

condition. As shown by Hertle [78], this indicates that $H - D$ is in the range of the Radon transform $\mathcal{R}$ [79,80]. As a consequence, one can define F such that:

$$H(x, \xi, t) - \mathbb{I}_{-\xi \leq x \leq \xi} D\left(\frac{x}{\xi}, t\right) = \int_\Omega \mathrm{d}\beta \mathrm{d}\alpha \, \delta(x - \beta - \alpha\xi) F(\beta, \alpha, t) \tag{43}$$

where $\Omega = \{(\beta, \alpha) \, | \, |\alpha| + |\beta| \leq 1\}$. Originally, F was introduced as a Double Distribution, independently by D. Mueller [6] and A. Radyushkin [7], while the D-term was originally introduced as a possible complementary tensorial structure to the DD F [81]. F was later identified as the Radon amplitude of the GPDs in ref. [82], and the formalism was further developed in ref. [83]. Finally, Equation (43) can be straightforwardly manipulated to obtain the well-known relation between GPDs and DDs:

$$H(x, \xi, t) = \int_\Omega \mathrm{d}\beta \mathrm{d}\alpha \, \delta(x - \beta - \alpha\xi)[F(\beta, \alpha, t) + \xi\delta(\beta)D(\alpha, t)]. \tag{44}$$

This result can be generalised to gluons, up to small modifications. In the nucleon case, the additional spin structure requires the introduction of an additional DD to describe the GPD E, but the D-term is the same between H and E up to a minus sign.

Finally, let us mention that the way to decompose the GPD between a Double Distribution and a D-term is not unique. This is a technical point and it has been discussed in the literature in detail (see [39,41,82,83]).

2.6. Positivity and Lightfront Wave Function Picture
2.6.1. The Lightfront Wave Function Picture

On top of polynomiality, another major property is associated with GPDs, called positivity. In order to properly understand such constraint discussed in several papers, we will introduce it though the Lightfront Wave Function formalism developed in [84].

To do so, we start decomposing the considered hadron states (here—the pion) in terms of LFWFs, labelled here $\Phi_\beta^{i\ldots j}$ such that:

$$|\pi\rangle \propto \sum_\beta \Phi_\beta^{q\bar{q}} |q\bar{q}\rangle + \sum_\beta \Phi_\beta^{q\bar{q},q\bar{q}} |q\bar{q}, q\bar{q}\rangle + \ldots \tag{45}$$

where the relevant quantum numbers are labelled with β and $^{i\ldots j}$ stands for the partonic content of the considered state. When a N partons state is considered, then the associated LFWFs depend on N lightfront momentum fractions x_i and N 2D transverse momenta $k_\perp^i$. The momentum conservation is guaranteed by three Dirac distributions.

Following the derivation given in great detail in ref. [84], one can express the matrix elements defining GPDs in Equations (2), (3), (9) and (10) in terms of an overlap of LFWFs. The interested reader can also look at examples of explicit computations in at leading Fock states (see, for instance, refs. [42,85]).

We will not reproduce these derivations here, and instead focus on the lightcone interpretation associated with considered kinematic area (see Figure 3), and its consequences on the overlap description. First, looking at the outer or DGLAP region, one obtains an overlap of LFWFs diagonal in terms of parton number N:

$$H^q(x, \xi)|_{x \geq \xi} \propto \sum_N \sqrt{1 - \xi^2}^{1-N} \sum_j \delta_{s_j, q} \int \left[\mathrm{d}x_i \mathrm{d}^2 k_\perp^i\right]_N \left(\Phi^N(\hat{r}_N)\right)^* \Phi^N(\tilde{r}_N) \delta(x - x_j), \tag{46}$$

where the measure is given as

$$\left[\mathrm{d}x_i \mathrm{d}^2 k_\perp^i\right]_N = \frac{1}{(16\pi^3)^{N-1}} \left[\prod_{i=1}^N \mathrm{d}x_i \mathrm{d}^2 k_\perp^i\right] \delta\left(1 - \sum_j x_j\right) \delta^{(2)}\left(\sum_j k_\perp^j\right) \tag{47}$$

in the $N \rightarrow N$ parton case [84]. The label j stands for the active partons, i.e., the one probed by the operator, while s_j is its flavour. The incoming and outgoing momenta degrees of freedom, boosted in the GPDs symmetric frame, are generically labelled with $\tilde{r}_N$ and $\hat{r}_N$, respectively. More details are provided in ref. [84].

From Equation (46), one realises that the overlap in the DGLAP region only includes convolution of LFWFs with the same number of partons. This is illustrated in Figure 5.
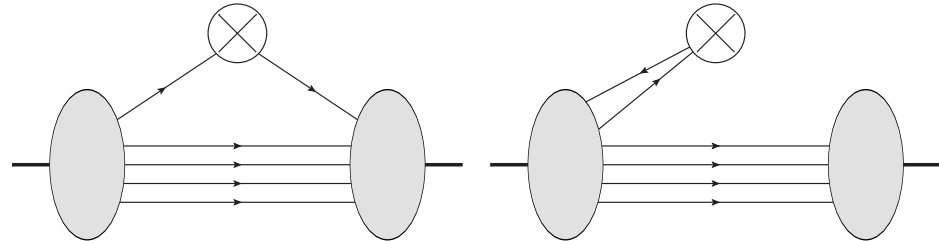

Figure 5. LFWFs decomposition of GPDs. **Left** panel, DGLAP region interpretation conserving parton number between incoming and outgoing states; **right** panel, ERBL region interpretation not conserving parton number as the incoming state emits a pair of quark–antiquark.

This contrasts with the ERBL region. There, a pair of quark–antiquark is extracted from the initial state and and contracted with the operator (see Figure 5). The overlap is off-diagonal in the Fock space and one obtains:

$$H^q(x,\xi)|_{x \leq |\xi|} \propto \sum_N \sqrt{1-\xi}^{2-N} \sqrt{1+\xi}^{-N} \sum_{j,j'} \frac{\delta_{\bar{s}'_j s_j} \delta_{s_j q}}{\sqrt{n_j n_{j'}}} \int \left[\mathrm{d}x_i \mathrm{d}^2 k_\perp^i\right]_{N-1}^{N+1} \delta(x-x_j)$$
$$\times \left(\Phi^{N-1}(\hat{r}_{N-1})\right)^* \Phi^{N+1}(\tilde{r}_{N+1}). \tag{48}$$

Similarly, the measure $\left[\mathrm{d}x_i \mathrm{d}^2 k_\perp^i\right]_{N-1}^{N+1}$ corresponds to the $N+1 \rightarrow N-1$ transition:

$$\left[\mathrm{d}x_i \mathrm{d}^2 k_\perp^i\right]_{N-1}^{N+1} = \mathrm{d}x_j \prod_{i \neq j,j'}^{N+1} \mathrm{d}x_i \delta\left(1-\xi-\sum_{i \neq j,j'}^{N+1} x_i\right) \frac{\mathrm{d}^2 k_\perp^j}{(16\pi^3)^{N-1}} \prod_{i \neq j,j'}^{N+1} \mathrm{d}k_\perp^i \delta\left(\frac{\Delta_\perp}{2} - \sum_{i \neq j,j'} k_\perp^i\right). \tag{49}$$

The discrepancy in terms of parton number between the initial and final state triggers ambiguity in the attempt to compute GPDs in the entire kinematic range at a given truncation of the Fock space. Thus, most of the time, only the DGLAP region is computed within models [42,86,87]. Nevertheless, modern solutions allow us to bypass this difficulty as we will discuss later on.

2.6.2. The Positivity Property

The LFWF picture in the DGLAP region allow us to derive an important property of GPDs called positivity. Focusing first on the forward case, when $\Delta \rightarrow 0$, one obtains:

$$q(x) \propto \sum_N \sum_j \delta_{s_j,q} \int \left[\mathrm{d}x_i \mathrm{d}^2 k_\perp^i\right]_N \left|\Phi^N(x_i, k_\perp^i)\right|^2 \delta(x-x_j). \tag{50}$$

The PDF q is expressed as the sum over momenta, partons content and quantum numbers of modulus square of the LFWFs. This is consistent with the probabilistic aspect of the PDF (number density) and a formal interpretation yielding PDF as the norm of a formal vector.

This structure can be generalised beyond the forward limit, to the entire DGLAP region. One formally recovers a scalar product in this parton number conserving kinematic area:

$$H(x,\xi)|_{x\geq\xi} = \langle\Phi_{\text{out}}|\Phi_{\text{in}}\rangle. \tag{51}$$

A simple Cauchy–Schwartz inequality yields:

$$|H(x,\xi)|_{x\geq\xi}| \leq |||\Phi_{\text{in}}\rangle|| \times |||\Phi_{\text{out}}\rangle||, \tag{52}$$

Plugging in the forward limit to describe the incoming and outgoing states, one obtains the positivity condition [84,88–91]:

$$|H^q(x,\xi)|_{x\geq\xi}| \leq \sqrt{q\left(\frac{x-\xi}{1-\xi}\right)q\left(\frac{x+\xi}{1+\xi}\right)}, \tag{53}$$

again, in the case of the pion. Small modifications appear in the nucleon case. The positivity property yields an upper and lower bounds on the GPD in the DGLAP region.

2.7. Scale Dependence and Evolution

2.7.1. Discussion in Momentum Space

As we have mentioned several times already, GPDs obey evolution equations, as the operators they are defined from need to be renormalised. Following ref. [92], the renormalisation of GPDs can be written as follows:

$$H^a(x,\xi,t,\mu^2) = \lim_{\varepsilon\to0}\int_{-1}^{1}\frac{\mathrm{d}y}{|y|}Z^{ab}\left(\frac{x}{y},\frac{\xi}{x},\alpha_s(\mu^2),\varepsilon\right)\hat{H}^b(y,\xi,t,\varepsilon), \tag{54}$$

where a,b stand for quark flavours q or gluon contributions. μ is the renormalisation scale, while ε is the regulator, ensuring that the bare operator remains finite. Since we use perturbation theory to describe the renormalisation properties of GPDs, our regularisation will be dimensional, such that $d = 4 - 2\varepsilon$. From Equation (54), one can apply a renormalisation group strategy to obtain:

$$\frac{\mathrm{d}H^a}{\mathrm{d}\ln\mu^2}(x,\xi,t,\mu^2) = \lim_{\varepsilon\to0}\int_{-1}^{1}\frac{\mathrm{d}y}{|y|}\frac{\mathrm{d}Z^{ab}}{\mathrm{d}\ln\mu^2}\left(\frac{x}{y},\frac{\xi}{x},\alpha_s(\mu^2),\varepsilon\right)$$
$$\times\int_{-1}^{1}\frac{\mathrm{d}z}{|z|}(Z^{bc})^{-1}\left(\frac{y}{z},\frac{\xi}{y},\alpha_s(\mu^2),\varepsilon\right)H^c(z,\xi,t,\mu^2), \tag{55}$$

i.e., the evolution equation of GPDs with respect to the scale μ. For the sake of completeness, let us highlight that Z^{-1} is defined such that:

$$\delta_{ij}\delta\left(1-\frac{z}{x}\right) = \lim_{\varepsilon\to0}\int_{-1}^{1}\frac{\mathrm{d}y}{|y|}(Z^{il})^{-1}\left(\frac{z}{y},\frac{\xi}{z},\alpha_s(\mu^2),\varepsilon\right)Z^{lj}\left(\frac{y}{x},\frac{\xi}{y},\alpha_s(\mu^2),\varepsilon\right). \tag{56}$$

The combination $\frac{\mathrm{d}Z}{\mathrm{d}\ln\mu^2}Z^{-1}$ can be seen as the momentum-dependent generalisation of the anomalous dimensions. Thus, we introduce the functions $\mathcal{P}$ such that:

$$\mathcal{P}^{ac}\left(\frac{x}{z},\frac{\xi}{x},\alpha_s(\mu^2)\right) = \lim_{\varepsilon\to0}\int_{-1}^{1}\frac{\mathrm{d}y}{|y|}\frac{\mathrm{d}Z^{ab}}{\mathrm{d}\ln\mu^2}\left(\frac{x}{y},\frac{\xi}{x},\alpha_s(\mu^2),\varepsilon\right)(Z^{bc})^{-1}\left(\frac{y}{z},\frac{\xi}{y},\alpha_s(\mu^2),\varepsilon\right). \tag{57}$$

Note that the function $\mathcal{P}$ is independent of ε, as the singularities are expected to cancel in the product $\frac{\mathrm{d}Z}{\mathrm{d}\ln\mu^2}Z^{-1}$, as we will explicitly see in the following in a one-loop expansion. Provided that Z can be computed non-perturbatively, one could obtain a description of the scale evolution. However, this has not been achieved yet, and the scale dependence of GPDs is computed perturbatively through the renormalisation group Equation (55). In the

$\overline{\text{MS}}$ scheme, letting implicit the factor $S_\varepsilon = \frac{(4\pi)^\varepsilon}{\Gamma(1-\varepsilon)}$ accompanying the polesin order to keep the notation simple, one can write:

$$Z^{ij}\left(\frac{x}{y}, \frac{\xi}{x}, \alpha_s(\mu^2), \varepsilon\right) = \delta_{ij}\delta\left(1 - \frac{x}{y}\right) + \sum_{n=1}^{\infty} a_s^n(\mu^2) \sum_{p=1}^{n} \frac{1}{\varepsilon^p} Z^{[n,p]}\left(\frac{x}{y}, \frac{\xi}{x},\right), \qquad (58)$$

where $a_s = \alpha_s/4\pi$. The derivative with respect to $\ln \mu^2$ is then given by:

$$\frac{dZ}{d\ln\mu^2}\left(\frac{x}{y}, \frac{\xi}{x}, \alpha_s(\mu^2), \varepsilon\right) = \frac{da_s}{d\ln\mu^2}(\mu^2)\frac{dZ}{da_s}\left(\frac{x}{y}, \frac{\xi}{x}, \alpha_s(\mu^2), \varepsilon\right)$$

$$= \left(-\varepsilon a_s(\mu^2) + \beta(a_s(\mu^2))\right)\left(\sum_{n=1}^{\infty} n a_s^{n-1}(\mu^2) \sum_{p=1}^{n} \frac{1}{\varepsilon^p} Z^{[n,p]}\left(\frac{x}{y}, \frac{\xi}{x},\right)\right), \qquad (59)$$

where we used the Renormalisation Group Equation (RGE) in $d = 4 - 2\epsilon$ dimension for the strong running coupling. Consequently, at leading order in a_s, $\mathcal{P}$ is given as:

$$\mathcal{P}^{ac}\left(\frac{x}{z}, \frac{\xi}{x}, a_s(\mu^2)\right) = -a_s(\mu^2)Z_{ac}^{[1,1]}\left(\frac{x}{z}, \frac{\xi}{x}\right). \qquad (60)$$

The one-loop result for $\mathcal{P}$ is thus finite, and can be computed in the $\overline{MS}$ scheme only from the pole contribution of the associated Feynman diagrams. Moreover, since $\mathcal{P}$ is only sensitive the UV-diverging part of the GPDs in $\overline{MS}$, it does not depend on the nature of the particle chosen at the level of the matrix element. Thus, one can perform the computations in a "partons-in-partons" approach, as it is performed in ref. [92]. In that case, some of the relevant Feynman diagrams at one loop in the lightcone gauge are shown on Figure 6.
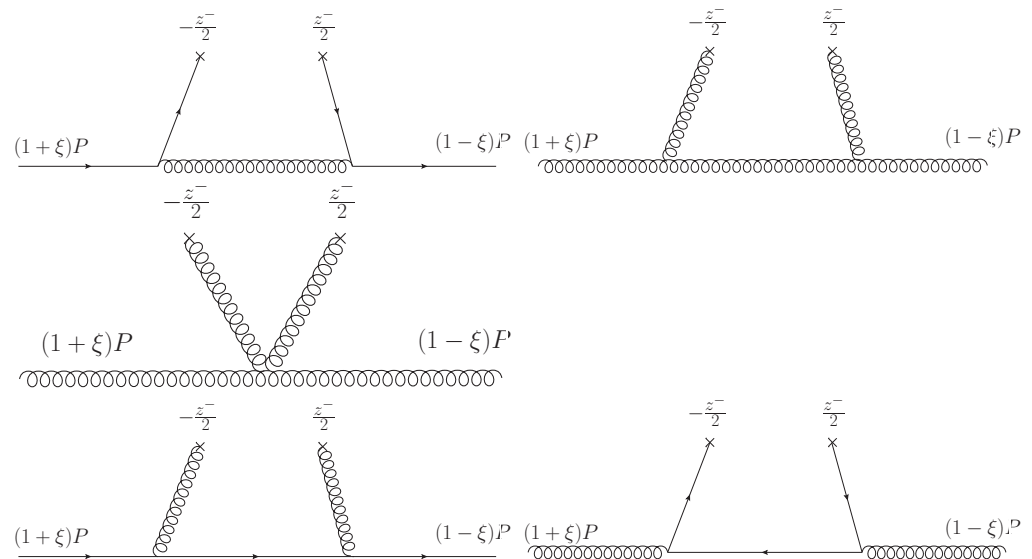

Figure 6. Feynman diagrams used to compute the one-loop anomalous dimension in the lightcone gauge. On the first and second lines, we display non-mixing terms, while the third line display diagrams mixing quark and gluon GPDs. On top of these connected diagrams, disconnected self-energy diagrams need to be added. In covariant gauges, additional contributions come from gluon exchanges with the Wilson line.

2.7.2. Properties of the Momentum-Dependent Anomalous Dimensions

The computation of the one-loop diagram leading to the one loop splitting function can be found in several papers [6,7,43,92]. We will adopt here the presentation of ref. [92]

to feed our discussion. Thus, for convenience, we assume in this section that $x > 0$ and we rewrite the evolution equation as:

$$\frac{\mathrm{d}H}{\mathrm{d}\ln\mu^2}(x,\xi,\mu^2) = \frac{\alpha_s(\mu)}{4\pi}\int_x^\infty \frac{\mathrm{d}y}{y}\mathcal{P}^\pm H^\pm\left(\frac{x}{y},\xi,\mu\right). \tag{61}$$

Here, the $\pm$ index correspond to the singlet and non-singlet combinations, already introduced in Equations (11) and (12), with the difference that the singlet is now a vector encompassing gluons:

$$H^+(x,\xi,\mu^2) = \begin{pmatrix} \sum_q H_q^+(x,\xi,\mu^2) \\ H^g(x,\xi,\mu^2) \end{pmatrix}, \tag{62}$$

and consequently, $\mathcal{P}^+$ is a matrix mixing quarks and gluons contributions:

$$\mathcal{P}^+(y,\kappa) = \begin{pmatrix} \mathcal{P}^+_{q\leftarrow q}(y,\kappa) & \mathcal{P}^+_{q\leftarrow g}(y,\kappa) \\ \mathcal{P}^+_{g\leftarrow q}(y,\kappa) & \mathcal{P}^+_{g\leftarrow g}(y,\kappa) \end{pmatrix}, \tag{63}$$

where we have introduced $\kappa = \xi/x$. One can then decompose $\mathcal{P}^\pm$ depending on the kinematics support of the contributions:

$$\mathcal{P}^\pm(y,\kappa) = \mathcal{P}_1^\pm(y,\kappa)\theta(1-y) + \theta(\kappa-1)\mathcal{P}_2^\pm(y,\kappa). \tag{64}$$

The explicit expressions of $\mathcal{P}_1^\pm$ and $\mathcal{P}_2^\pm$ are given in ref. [92]. Here we see that the $\mathcal{P}_2^\pm$ contributes only for $\xi > x$. Thus, when $\xi = 0$, only $\mathcal{P}_1^\pm$ contributes in the entire y range, and reduces to the DGLAP splitting functions. Hence, the name of the $\xi < x$ kinematic region. In the kinematics region where $x < \xi$ both $\mathcal{P}_1^\pm$ and $\mathcal{P}_2^\pm$ contribute. The transition between the two regions is continuous as $\lim_{\kappa\to 1}\mathcal{P}_2^\pm(y,\kappa) = 0$, but due to the presence of the θ function, it is not smooth. In fact, the evolution kernel will generate a cusp at $x = \pm\xi$ when evolving smooth GPDs functions. This contrasts with the claim sometimes made in the literature that evolution smoothens the behaviour of GPD models on the $|x| = |\xi|$ lines (by rendering a discontinuous GPDs model at low scale continuous at higher scales for instance).

Finally, let us mention that in momentum space, only two evolution codes at leading order are publicly available, the Vinnikov code [93], which is not maintained anymore, and Apfel++ [94–96]. Both of them are integrated through the PARTONS framework [97].

2.7.3. Evolution in Conformal Space

An alternative picture to momentum space evolution is provided by moments, or conformal space evolution. The idea originated from the expansion of a non-local operator into a set of local ones through operator product expansion (OPE). The local operators involved in the expansion need to be renormalised and thus, all of them obtain an "a priori" different renormalisation scale dependence. The original non-local operator and its scale dependence can then be recover by resumming the renormalised local operators.

In the PDF field, this is typically what is done when one performs the evolution through the Mellin moments before applying the inverse Mellin transform. In the GPD case, as the splitting functions are more complicated, the situation is not as simple. The Mellin moments mix under GPD renormalisation, making their evolution and resummation more involved. However, it is possible to diagonalise the basis of local operator for a given order of perturbative evolution. At order α_s, the evolution operator commutes with the conformal symmetry operators, which tells us that both operators can be diagonalised on the same basis [98]. From that, one deduces that the conformal moments, defined in the non-singlet sector as

$$\mathcal{C}_n^-(\xi,t,\mu^2) = \xi^n\int_{-1}^1 \mathrm{d}x\, C_n^{3/2}\left(\frac{x}{\xi}\right)H^-(x,\xi,t,\mu^2), \tag{65}$$

where $C_n^{3/2}$ are the 3/2-Gegenbauer polynomials of order n, do not mix among each other. In the limit when $\xi \to 0$, the conformal moments reduce to the Mellin one, consistently with the evolution kernel going to the DGLAP one. In the case when $\xi \to 1$, the Gegenbauer polynomial formed a base in x of the GPD support, and one recovers the diagonalisation of the evolution kernel à la "Efremov-Radyushkin-Brodsky-Lepage". The conformal moments obey an evolution equation of the type of:

$$\frac{\mathrm{d}\mathcal{C}_n^-}{\mathrm{d}\ln\mu^2}(\xi,t,\mu^2) = \frac{\alpha_s(\mu)}{4\pi}\mathcal{V}_n\mathcal{C}_n^-(\xi,t,\mu^2), \tag{66}$$

where

$$\mathcal{V}_n = 2C_F\left(\frac{3}{2} + \frac{1}{(n+1)(n+2)} - 2\sum_{k=1}^{n+1}\frac{1}{k}\right) \tag{67}$$

with $C_F = 4/3$. The solution of this equation is given as:

$$\mathcal{C}_n^-(\xi,t,\mu^2) = \left(\frac{\alpha_s(\mu^2)}{\alpha_s(\mu_0^2)}\right)^{-\frac{\mathcal{V}_n}{\beta_0}}\mathcal{C}_n^-(\xi,t,\mu_0^2) \tag{68}$$

where β_0 is the leading order term of the QCD β function given as $\beta_0 = 11 - 2/3 * n_f$, where n_f is the number of active quark flavours. From Equation (68), one can note the advantage of moments evolution, which is purely multiplicative, and not convoluted as in momentum space. However, the difficulties lie in the reconstruction of the x-dependent function. Indeed, the Gegenbauer polynomials introduced in (65) do not form an orthogonal basis for $x \in [-1,1]$ but $x \in [-\xi,\xi]$, complicating the evolution of a polynomial expansion of GPDs. Moreover, such an expansion is expected to converge very slowly and thus, resumming techniques have been introduced relying on Mellin–Barnes integrals [99]. The Mellin–Barnes integral transform requires knowledge of the conformal moments for $n \in \mathbb{C}$ and not just integer values. Thus, an analytic continuation of the moments within the complex plane is required, and if the moments are not given by an algebraic formula, this continuation can be challenging. Moreover, its uniqueness is not guaranteed. Nevertheless, models in conformal space have been developed [100,101] and are today among the most successful ones.

In the singlet sector, mixing between quarks and gluons is unavoidable for a given order n of the conformal moments. Gluon conformal moment distribution follows the same definition as in (65), but is computed from 5/2-Gegenbauer polynomials $C_n^{5/2}$. An additional diagonalisation of the 2×2 matrix is necessary. An example is given in the specific case of the D-term in ref. [71].

Finally, let us briefly discuss what happens beyond leading order. Evolution kernels have been derived at two loops (and at three loops in the non-singlet case) [102–107]. In the $\overline{\mathrm{MS}}$ scheme, the conformal moments $\mathcal{C}_n$ start mixing among each other in such a way that:

$$\mathcal{C}_n(\mu^2) = \sum_{j=0}^{n} b_{nj}(\mu^2,\mu_0^2)\mathcal{C}_j(\mu_0^2), \tag{69}$$

yielding a triangular matrix at a given order n (see [108]). This complicates the evolution and reconstruction in x-space of NLO evolved GPDs in conformal space. Consequently, in $\overline{\mathrm{MS}}$, the strategy is rather to evolve Wilson coefficients in the computation of a process rather then the GPD itself (see, e.g., [100]). An alternative solution is to work in a specific scheme in which the off-diagonal coefficients vanish. This scheme is labelled conformal scheme (or $\overline{\mathrm{CS}}$), and is defined so that in the forward limit, one recovers the $\overline{\mathrm{MS}}$ scheme results (this is possible as PDFs Mellin moments do not mix under evolution). This specific scheme has allowed early descriptions of DVCS at NNLO accuracy [100], before modern computations in $\overline{\mathrm{MS}}$ scheme [109]. From the first studies on scheme dependence [100],

the difference between $\overline{CS}$ and $\overline{MS}$ is mild for the quarks, and somehow more sizeable for gluons, while NLO and NNLO quark GPDs are indistinguishable.

3. Continuum Results for Mesons

3.1. Impulse Approximation and Its Limitations

In the meson sector, one of the first attempts to compute GPDs (see, e.g., [110–112]) relied on the so-called impulse approximation, graphically represented in Figure 7.
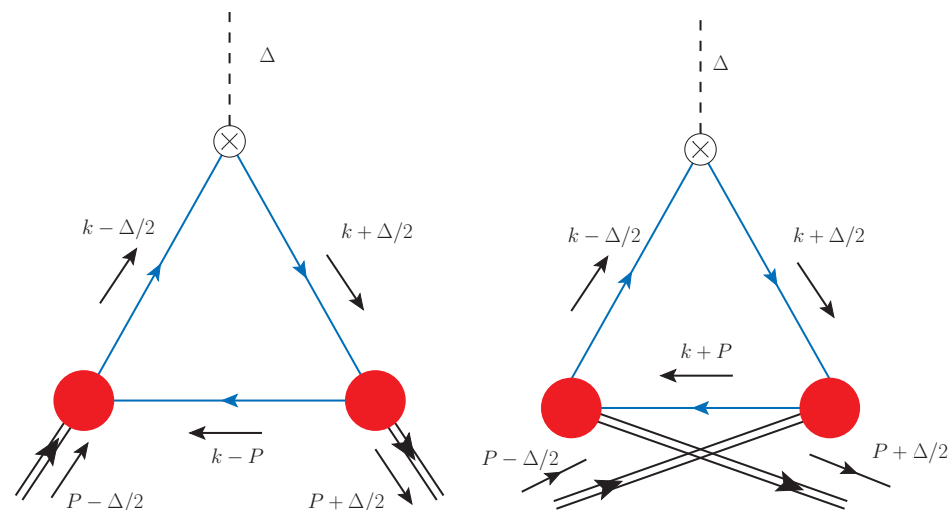

Figure 7. Triangle diagrams used in early computations of meson EFF, PDFs and GPDs.

In this framework, a pion is split into a quark–antiquark pair and is later reformed. In between, one computes the impact of local twist-two operators defined in Equation (37) inserted within a quark line. Using this technique, one gains access to the Mellin moments of the GPDs (including the D-term contribution), and thus, a reconstruction technique is necessary to gain access to the x-dependence of the distribution. If polynomials reconstructions have been tried (see, e.g., refs. [42,113]), direct identifications of Double Distributions has been favoured in the literature [60,112,114].

Such computations rely on two main points:

- The computation (or modelling) of non-perturbative QCD correlation functions such as the Bethe–Salpeter wave function, the quark propagator and the local operator;
- The validity of the impulse approximation.

We will not enter here the discussion about the consistent computation of the non-perturbative QCD correlation function, and instead, we redirect the reader toward a previous review paper [42] and refined studies of the pion Bethe–Salpeter wave function performed since then [115,116]. Rather, we will discuss the limitations of the impulse approximation.

When one chooses an approximation set such that the Bethe–Salpeter amplitude is independent of the relative momentum (k in Figure 7) the forward limit of the GPD, i.e., the PDF, ends up being symmetric with respect to $x \to 1 - x$, as expected from momentum conservation in the two-body case. However, as soon as the Bethe–Salpeter amplitude becomes k dependent, the momentum conservation and the two-body symmetry are lost (see for instance [117]). This is a consequence of missing contributions in the computation of matrix element of local twist-2 operators. Loosely speaking, as the relative momentum dependence kicks in, the Bethe–Salpeter amplitude gains a spatial extension. Thus, the operator can be inserted "within" the amplitude. This idea yields additional contributions as illustrated in Figure 8.
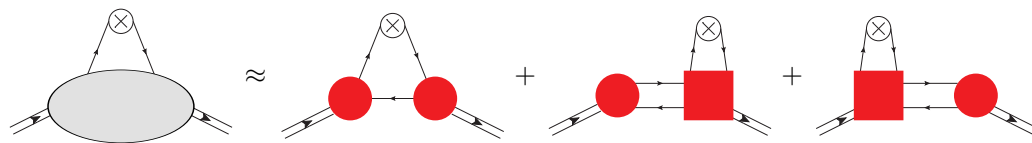
Figure 8. Decomposition of contributions to the local operators when the Bethe–Salpeter amplitude is momentum-dependent. The red circles correspond the standard Bethe–Salpeter amplitudes, while the squares include modifications allowing the insertion of the local operators.

As shown in [42,113,114], in the Rainbow ladder approximation, the new contributions can be written in terms of the Bethe–Salpeter amplitude Γ_π as:

$$\text{} = -\frac{1}{2}(k \cdot n)^m n^\nu \frac{\partial \Gamma_\pi}{\partial k^\mu}(k, P), \tag{70}$$

where n is a lightlike vector so that $k \cdot n = k^+$ and m is the order of the Mellin moment considered.

The impact of the additional terms is shown in Figure 9 in the case of simple algebraic models for the Bethe–Salpeter amplitudes and the quark propagators (see [42,113,114]). Being anti-symmetric with respect to $x \to 1 - x$, it does not contribute to the PDF normalisation. It exactly compensates the antisymmetric component of the triangle contribution alone, restoring the symmetry of the complete result. The most advanced computations using this technique can be found in [118].
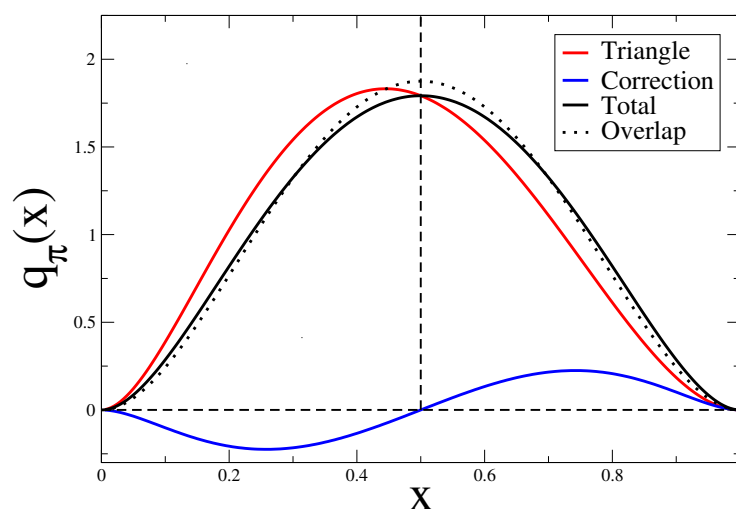

Figure 9. Results for the forward limit after reconstruction of the x-dependence in the case of a simple, algebraic model (see [42,113,114]). The total PDF (solid black) is symmetric under $x \to 1 - x$ transformation, but the sole triangle diagram contribution (solid red) is not. The additional terms coming from the square vertices in Equation (70) provide the adequate correction (solid blue).

If this contribution allows one to recover the expected symmetry properties in the forward limit, it remains insufficient for tackling GPD computations in the entire kinematic domain. More precisely, at non-vanishing skewness, the additional vertices in Equation (70) are not able to restore the positivity property. As the forward limit yields a symmetric and thus vanishing contribution at small-x, the positivity property imposes that the GPD is also vanishing at $|x| = |\xi|$. Models employing momentum-dependent Bethe–Salpeter have thus been limited to the vanishing ξ kinematic region [60]. Note that models based

on the Nambu–Jona–Lasinio (NJL) approximation are not impacted, since the amplitude is momentum-independent [119–121]. However, in the NJL approximation, the triangle diagram is not sufficient in off-forward kinematics as the meson resonances appear in the *t*-channel, contributing to the *D*-term [119,122,123]. Thus, omitting the resonances leads to a breaking of the soft pion theorem in the chiral limit. To go beyond vanishing skewness, techniques based on LFWFs have been developed.

3.2. From Bethe–Salpeter Wave Funtions to Lightfront Wave Functions

As we highlighted previously, the most natural way to fulfil the positivity property is to start modelling GPDs as overlaps of LFWFs. Different techniques exist to compute the LFWFs, from Lightfront Hamiltonian (see, for instance, [124]) to ADS/QCD (e.g., refs. [86,125]). We will focus here on the connection between the Bethe–Salpeter and Lightfront wave functions, in the case of the pion.

The *N*-body Bethe–Salpeter wave function can be projected out to obtain all the independent *N*-body LFWFs carrying the quantum numbers of interest (mostly the helicity projection of the quark, and thus the orbital angular momentum projection of the pion). If nothing forbids the computation of *N*-body Bethe–Salpeter wave function, in practice, today, only the two-body one is computed as it involves only four-point functions. Thus, we will further restrain ourselves to the lowest Fock state of the pion.

The two-body LFWFs Φ for the pion are given as projection of the Bethe–Salpeter wave function χ_π. The latter is defined by "attaching" quark propagators to the Bethe–Salpeter amplitude: $\chi_\pi = S\Gamma_\pi S$. The connection the the LFWFs is then given through (see, for instance, [126]):

$$P^+ \Phi_{\uparrow\downarrow}(x, k_\perp) = \int \frac{dk^-}{2\pi} \mathrm{Tr}\left[\gamma^+ \gamma_5 \chi_\pi(k, P)\right], \tag{71}$$

$$2ik^i P^+ \Phi_{\uparrow\uparrow}(x, k_\perp) = \int \frac{dk^-}{2\pi} \mathrm{Tr}\left[\sigma^{+i} \gamma_5 \chi_\pi(k, P)\right], \tag{72}$$

where $\uparrow\downarrow$ and $\uparrow\uparrow$ indicate the helicity projection of the quarks. If the projection looks simple, it is in fact made complicated by the lightcone integration over k^-, as the Bethe–Salpeter wave function is typically computed in Euclidean space, using standard euclidean variable. This difficulty is usually bypassed by using spectral, or Nakanishi representation [30,31] for the Bethe–Salpeter amplitude Γ_π in Euclidean space:

$$\Gamma_\pi(k, P) = \int_0^\infty d\omega \int_{-1}^1 dz \frac{\rho(z, \omega)}{\omega + \left(k + \frac{z}{2}P\right)^2}. \tag{73}$$

The advantage of this representation is that the momenta degrees of freedom can be algebraically manipulated, while the non-perturbative information is shifted toward the Nakanishi weight ρ. Different modelling strategies have been performed in the literature, from simple algebraic Ansätze [60,127] to parametric fit [128,129] or even direct computations in the specific case of QED N-point functions [130]. The results obtained in the forward limit are similar to those obtained through the diagrammatic computation, as shown by the dotted line on Figure 9 in the case of the simple algebraic model of [42]. Concerning GPDs computations, only algebraic Ansätze and parametric fits have been used.

As the reader may have noted, the fact that only the two-body LFWFs are available from the two-body Bethe-Salpeter wave function make the computation of the GPDs possible only in the DGLAP region, as the first term in the ERBL one would require the four-body LFWFs. Thus, a priori, if positivity is well fulfilled, it is not possible to complete polynomiality, as DGLAP and ERBL contributions are intertwined to yield polynomials Mellin moments. Such a hole in the kinematic domain has to be filled and we will see how in the next section. Nevertheless, accessing the DGLAP region alone remains highly valuable. Indeed, it gives access to the PDF when $\Delta \to 0$, while EFF can be recovered after integrating over x at $\xi = 0$. Furthermore, the 3D density interpretation is also accessible from the

DGLAP region only. The major missing part is the EMT for factor *C* of Equation (21), and more generally, the *D*-term of Equation (40).

As highlighted in [59], under specific assumption on the Bethe–Salpeter wave function, the associated LFWFs ends up being separable between x and $k_\perp$ variable so that:

$$\Phi(x, k_\perp) = \varphi(x)\psi(k_\perp). \tag{74}$$

This separability property triggers interesting simplifications. First, φ yields the pion distribution amplitudes, up to a normalisation constant. Then, the PDF computed as an overlap of LFWFs in Equation (50) becomes proportional to the square of the pion distribution amplitude. Regarding GPDs, this factorisation yields the following functional form [58,85]:

$$H_\pi(x, \xi, t) = \sqrt{q_\pi\left(\frac{x - \xi}{1 - \xi}\right) q_\pi\left(\frac{x + \xi}{1 + \xi}\right)} \Psi_\pi(x, \xi, t), \tag{75}$$

where $\Psi < 1$. The positivity property is thus manifestly fulfilled, as expected starting from a LFWF description of the nucleon. This formula is used in ref. [58] to introduce new kinds of models, exploiting PDFs computed in the covariant approach, but beyond the impulse approximation [118]. The Ψ can be then modelled or computed following the simple Anzätze or parametric fits available. Under two assumptions regarding the Nakanishi parametrisation: (i) the hadron mass can be neglected and (ii) the ω dependence of the weight ρ can be approximated by a Dirac delta, Ψ can be written as:

$$\Psi(x, \xi, t) = \Psi(z), \quad \text{with} \quad z = -t\frac{(1 - x)^2}{1 - \xi^2}. \tag{76}$$

Introduced in ref. [85], this simplification has been exploited in refs. [59,129].

The computations in the DGLAP region allow one already to extract valuable information, and in particular, the impact parameter space density $\rho(x, b_\perp)$. Regarding that point, realistic computations start emerging in the literature based one the Nakanishi representation (see refs. [59,87]). Consequently, computations of the 1+2D densities, both for the pion and kaon, have been obtained using different modelling techniques for the Nakanishi weight, or for the LFWFs themselves. The results presented in Figure 11 of ref. [59] highlight the differences that can be expected from different modelling strategies of the LFWFs. They are sizeable, especially in the kaon case.

3.3. The Covariant Extension

Even if the modelling of GPD in the DGLAP region only provides interesting outcomes, it precludes any comparison with potential future experimental data, as part of the kinematic range, the ERBL region, is missing. Since the two-body Bethe–Salpeter wave function allows us only to recover the two-body LFWFs, the standard overlap representation in the ERBL region is out of reach, and would anyway lead to a GPD model violating the polynomiality property. Consequently, another strategy should be sought.

The answer was provided few years ago, exploiting the Radon transform property existing between GPDs and DDs (see Equation (43) and ref. [83]). This technique, labelled covariant extension, allows one to exploit both the LFWFs formalism, and the DDs one, guaranteeing by construction that all GPDs theoretical properties are fulfilled. This work followed a pioneering example given in [131], and can be connected with the Laplace transform [132]. The key point of the covariant extension is to exploit the properties of the inverse Radon transform. More precisely, Boman and Todd–Quinto showed that compactly supported distributions can be reconstructed from a partial knowledge of their Radon transform [133]. In the case of GPDs, this can be translated as such: the knowledge of the GPD in the DGLAP region is sufficient to reconstruct uniquely the Double Distribution

F introduced in Equation (43) [83] (in fact, even an incomplete knowledge of the DGLAP region is enough [134]).

Since the proof presented in refs. [83,133] is rather technical, we will not enter the details here. Rather, we will provide the reader with an intuitive picture relying on tessellation and finite element methods. As illustrated in Equation (43), the Radon transform consists in integrating a function along lines. As illustrated on the left-hand side of Figure 10, the DGLAP and ERBL lines are different to the former cross the $\beta = 0$ axis outside of the definition domain, while the ERBL one hit this line within the the DD support. Looking at the right-hand side of Figure 10, one can discretise the support of the DD (only the upper right corner is shown because of symmetry properties in α and β). A DGLAP-type line is shown, probing a given number of cells. It is easy to realise that each cell can be probed by infinitely many DGLAP lines, and that reducing the size of the cell does not modify this statement. Thus, every point on the DD support, expect the one such that $\beta = 0$, is probed by infinitely many DGLAP lines. This provides the level-arm to recover the DD *F* from the DGLAP region only. However, it does not allow recovering the *D*-term, which remains inaccessible (some specific Double Distribution schemes allow one to extract a *D*-term, but the latter remains ambiguous [83,135]).
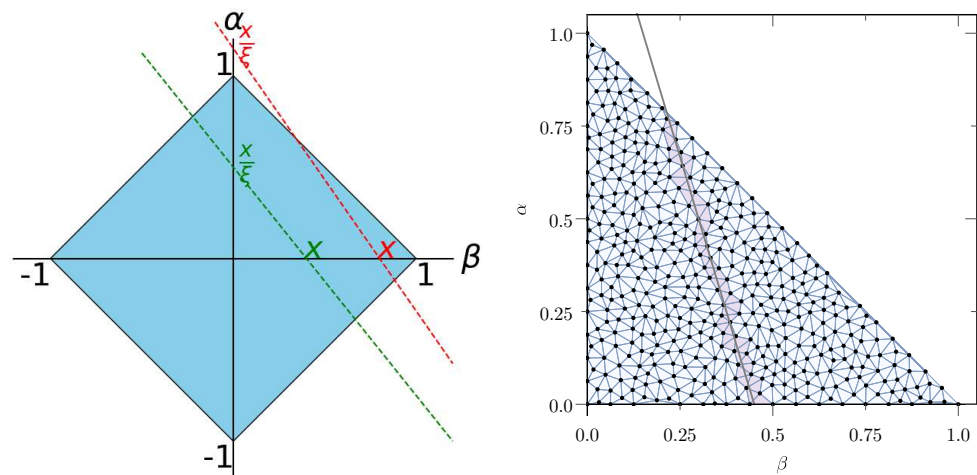

Figure 10. Left: Support of the DD and example of a DGLAP line (red) and ERBL line (green). **Right**: Support of the DD *F* after tessellation using a Delaunay mesh. An example of a DGLAP line is given. If numerous enough, those lines can probe every cell of the DD support. Figure from [58].

Figure 10 also highlights another difficulty in any attempt to recover the DD from the GPD in the DGLAP region only. Indeed, if one wants to probe the region close to the point $(0,0)$ in the (β, α) space, the associated DGLAP lines become almost parallel, and yields a badly conditioned inverse problem. In fact, the Radon inverse problem is known to be ill-defined in the sense of Hadammard [136–138], since, even before discretisation, the Radon transform is not continuous. The discretisation makes the problem worse, as the existence and uniqueness of a solution is not guaranteed anymore, requiring regularisation techniques to ensure the convergence of reconstruction algorithms. In the following, we will discuss the strategy applied in ref. [58].

The discretised problem can be expressed as looking for a DD vector *F* such that:

$$\begin{pmatrix} H_i \end{pmatrix} = \begin{pmatrix} \mathcal{R}_{ij} \end{pmatrix} \begin{pmatrix} F_j \end{pmatrix}, \tag{77}$$

where $\mathcal{R}$ is the matrix of the discretised Radon transform and H_i—a given sample of the GPD in the DGLAP region. The size of the vector *F* is a function of the number of cells introduced for the discretisation, but also the degree of the polynomials used to

approximate locally the Double Distribution. The elements F_j are taken at a position (β_j, α_j), which depends on the polynomial order and is called a node. For instance, a zero-order polynomial interpolation requires a node at the barycentre of each cell, while a degree-one interpolation requires a node at every vertex of the mesh. On the left-hand side, the size of H depends of the available sampling of the GPD in the DGLAP region. At minimum, the size of H_i should be as large as F_j, allowing the rank of the matrix $\mathcal{R}$ to be maximal, and thus, the problem invertible.

However, the solution of Equation (77) might be rather sensitive to the initial conditions such as the shape and size of the grid, or the sampling of the GPD. To overcome this difficulty, one can overconstrain the system by having $\mathcal{R}$ have more lines that columns, and look for a solution through a least-squares strategy. To do so, an adequate strategy is to use the so-called normal equations, although direct least-squares algorithms such as LSMR [139] can be used [83]. Rather than using iterative algorithms to minimise the associated χ^2, the normal equations provide directly the minimal solution F_j. The normal equations transform our linear system (77) into

$$F = \left(\mathcal{R}^T \mathcal{R}\right)^{-1} \mathcal{R}^T H. \tag{78}$$

In addition, it allows to simply propagate uncertainties on the values of H in that DGLAP region onto the ERBL one after the reconstruction through the DD. This is based on computations of the covariant matrix (see [58,140] for details).

In practice, for a simple functional form of DD F from ref. [85]:

$$F(\beta, \alpha) = \frac{15}{2} \theta(\beta) \left(1 - 3(\alpha^2 - \beta^2) - 2\beta\right), \tag{79}$$

an excellent agreement can be obtained through the reconstruction procedure for 780 cells and furst-order Lagrange polynomials. The results are illustrated in Figure 11, highlighting the good control on the uncertainties in the ERBL region through the reconstruction. Note however that even if the functional form is simple, the model is made more complicated by the specific DD scheme labelled Pobylitsa (or P) scheme, in which it is defined.
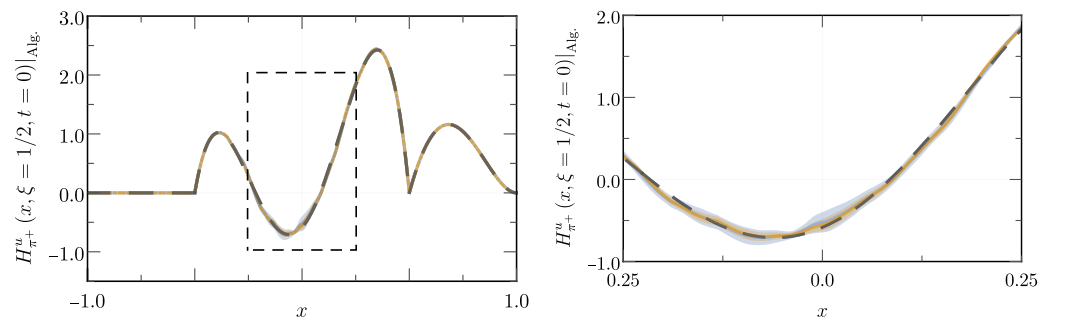

Figure 11. Left: results of the reconstuction of the DD of Equation (79). Black, exact GPD computed from the algebraic DD (79). Blue, reconstructed GPDs with a sample of H_i roughly four times the number of cells. Orange, same but with a sample of 12 times the number of cells. **Right**: zoom on the central region to highlight the uncertainty bands.

This technique, together with the simplified assumption of Equation (75), has been used to build "theoretically complete" models of the pion GPDs, ensuring that both polynomiality and positivity were fulfilled by construction, and based on state-of-the-art computations of the pion PDF using continuum techniques. The next step is to assess whether these sophisticated models of GPDs could one day be compared to experimental data.

3.4. The Sullivan Process

As we mentioned earlier, GPDs can be probed in deep exclusive processes. These processes require a high luminosity of the experimental set up. However, there is no facility

today with a high enough luminosity allowing to make exclusive experiments through real pion targets. One thus has to find another solution.

3.4.1. Introduction to the Sullivan Process

Since the 1970s, one of the main ideas for studying the internal structure of the pion is to rely on the so-called Sullivan process [141], i.e., to hit a virtual pion within the meson cloud of the nucleon. It has been used to probe the pion EFF [142–144] and also the pion PDFs [145,146]. In order to probe GPDs, one focuses on the best-understood process, namely, Deep Virtual Compton Scattering (DVCS). The latter describes the exclusive electroproduction of a photon out of a pion, the latter remaining intact. This is illustrated on the left-hand side of Figure 12.
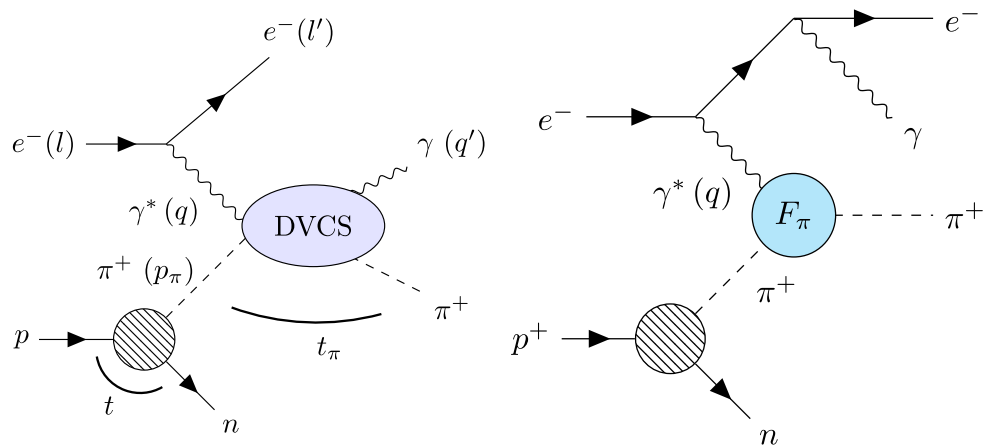

Figure 12. Left: Sullivan DVCS $ep \rightarrow en\gamma\pi^+$. At small t, one expects the pion pole contribution to be the leading one in such a process. **Right**: Sullivan Bethe–Heitler, interfering with the DVCS.

The differential cross section of the complete process $d\sigma_{Sul}$ depends on multiple kinematic variables [147]. Among the lists are the photon virtuality $Q^2 = -q^2$, the fraction of energy carried by the virtual pion $x_\pi = p_\pi \cdot l/(p \cdot l)$ and the inelasticity of the process $y = p \cdot q/p \cdot l$. Three angles are also necessary to characterise the kinematics in the laboratory frame. The first is ϕ, the angle between the leptonic plane (formed by the incoming and outgoing electrons), and the hadronic plane (formed by the virtual photon and the outgoing pion). The two others are the azimutal angle of the outgoing electron ϕ_e and of the outgoing neutron ϕ_n. The subprocess $e\pi \rightarrow e\pi\gamma$ is characterised by related subkinematic variables such as the inelasticity of the subprocess $y_\pi = p_\pi \cdot q/p_\pi \cdot l$ or the Bjorken variable of the subprocess $x_B^\pi = Q^2/(2p_\pi \cdot q)$. Then, one can write the differential cross section of the Sullivan process in terms of the subprocess differential cross section [147,148] as:

$$\frac{d^8\sigma(\lambda, \pm e)}{dydQ^2 dt_\pi d\phi d\phi_e dx_\pi dt d\phi_n} = x_\pi \frac{g_{NN\pi}^2}{16\pi^3} F(t, \Lambda^2)^2 \frac{-t}{(m_\pi^2 - t)^2} |J_{x_B^\pi}^{Q^2}| \frac{d^5\sigma^{e\pi \rightarrow e\pi\gamma}(\lambda, \pm e)}{dy_\pi dx_B^\pi dt_\pi d\phi d\phi_e}, \quad (80)$$

where λ is the longitudinal polarisation of the electron beam, e—the electron charge, $g_{NN\pi}$—the pion-nucleon coupling, and $F(t, \Lambda)$—the associated form factor. Following ref. [147], a single-parameter functional form is chosen:

$$F(t, \Lambda) = \frac{\Lambda^2 - m_\pi^2}{\Lambda^2 - t} \quad (81)$$

with $\Lambda = 800$ MeV. $|J_{x_B^\pi}^{Q^2}|$ is the Jacobian between Q^2 and x_B^π. To be valid, the Sullivan process requires that the pion pole contribution dominates, and thus, that t remains small enough. Additionally, the Bjorken regime is achieved at the level of the subprocess for both Q^2 and $s_\pi = (p_\pi + q)^2$ large in front of other scales involved.

However, DVCS on a virtual pion is not the only process contributing to the $ep \rightarrow en\gamma\pi^+$ cross section. Additional N^* resonances decaying in the $n\pi$ channel can interfere with the Sullivan process. Their impact is reduced by ensuring that the invariant mass between the neutron and pion is large enough, typically larger than 2 GeV. However, one process always interfere with the DVCS one, the Bethe-Heitler process, shown on the right-hand side of Figure 12. Being a QED process and depending only of the pion EFF, the Bethe–Heitler contribution is computable, usually larger than the DVCS one and through the interference term, it magnifies the impact of GPDs. The subprocess cross section is thus decomposed in terms of amplitudes $\mathcal{T}$ as:

$$\frac{\mathrm{d}^5\sigma^{e\pi \rightarrow e\pi\gamma}(\lambda, \pm e)}{\mathrm{d}y_\pi \mathrm{d}x_B^\pi \mathrm{d}t_\pi \mathrm{d}\phi \mathrm{d}\phi_e} = \frac{\alpha_{QED}^3 x_B^\pi y_\pi}{16\pi^2 Q^2 \sqrt{1+\epsilon^2}} \frac{|\mathcal{T}^{BH}|^2 + |\mathcal{T}^{DVCS}|^2 \mp \mathcal{I}}{e^6}, \tag{82}$$

where the interference term is further decomposed in $\mathcal{I} = \mathcal{I}_{unpol} + \lambda\mathcal{I}_{pol}$, α_{QED} is the electromagnetic coupling and $\epsilon = (2m_\pi x_B^\pi)^2/Q^2$.

3.4.2. From the Sullivan Process to GPDs

The amplitude $\mathcal{T}^{DVCS}$ and interference term $\mathcal{I}$ are not directly parametrised in terms of GPDs, but rather in terms of Compton Form Factors (CFFs) $\mathcal{H}$ which are connected to GPDs through:

$$\mathcal{H}(\xi, t, Q^2) = \int_{-1}^1 \frac{\mathrm{d}x}{\xi} C\left(\frac{x}{\xi}, \frac{Q^2}{\mu^2}, \alpha_s(\mu^2)\right) H(x, \xi, t, \mu^2), \tag{83}$$

where C is a coefficient function, computed in perturbation theory. The decomposition of the DVCS amplitude and the interference term as a function of the CFFs can be found in ref. [149]. Rather than looking at the exact expression, we will assume for a moment that experimental data allow us to extract with a great accuracy $\mathcal{H}$ and ask whether it is possible to inverse the convolution of Equation (83) to regain the GPD H.

The answer to this question has been known for a long time if C is computed and the leading order of α_S only, and it is "no". In fact, at leading order, any GPD such that $H(\xi, \xi, t, \mu^2) = 0$ yields a vanishing CFF, and is thus invisible in experimental data. It was thought that this problem would vanish a once higher order of perturbation theory or evolution equations would be turned on [150]. This has been proven wrong in [151], where the concept of shadow GPDs is introduced. Briefly shadow GPDs are constructed so that below an given order of perturbation theory n, the associated CFFs vanish, and that their forward limits also vanish. Consequently, they are invisible both in DVCS and DIS. Of course, the exact cancellation is valid only at a fixed scale μ_{shadow}, but it was also shown that evolution has little effect on improving the situation [151].

In the case of the nucleon, the way out is to go through multichannel analysis of GPDs, as shadow GPDs are process dependent, i.e., a shadow GPD for DVCS can be visible in another process. In fact, some processes are expected to be free of shadow GPDs, such as Double DVCS [152]. However, these processes are much harder to measure already in the nucleon case, and are thus out of reach for the pion through the Sullivan process. In the case of the pion, rather than extracting GPDs from experimental data, the aim is to challenge existing models through comparison of predictions of the Sullivan process observables, with potential future measurements.

The first step in that direction is to figure out whether or not present and future facilities will be able to measure enough events connected to the Sullivan process. To assess that, we used a theoretically complete model of GPDs, fulfilling all required theoretical properties, and computed the CFFs associated with that model in ref. [58], using the PARTONS software [97] using a next-to-leading order description of the coefficient function, and computed separately quarks and gluon contributions. The result is illustrated in Figure 13, where the theoretically complete model corresponds to the brown curve. One can note an interesting characteristic, the sign of the real and imaginary part of the CFF changes with

the inclusion of gluons. This is understood as the quark and gluon contributions to the CFF comes with a relative minus sign. This behaviour is confirmed, and even strengthened at next-to-next-to-leading order (N2LO) [153]. Thus, generally speaking, the sign of the CFF indicates the relative strength between quark and gluon contribution. Accessing such a sign would already favour or disfavour different pion GPD models.
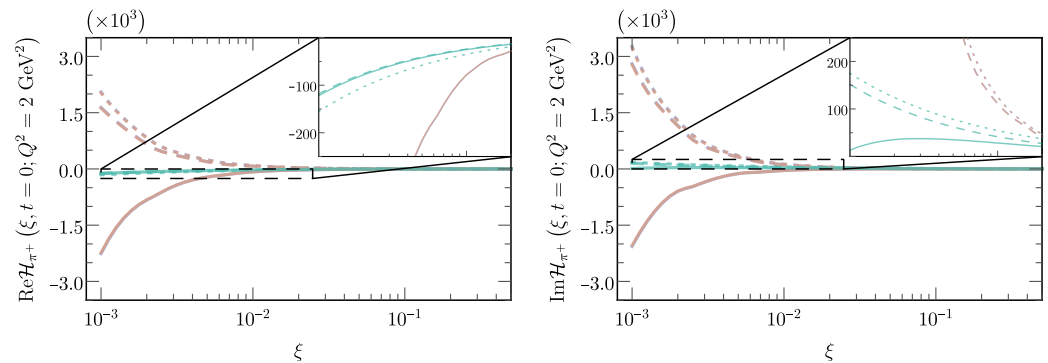

Figure 13. Real (**left**) and imaginary (**right**) parts of DVCS Compton Form Factors computed with theoretically complete model developed in ref. [58] (brown curves). Dotted lines correspond to LO computation, dashed lines—to NLO without gluon contributions and the solid lines to the full NLO computation. The light blue curves are built from standard phenomenological Ansätze in the GPD framework [55], and a phenomenological forward limit [58,154] for details).

3.4.3. A Smoking Gun for Gluons at the EIC and EicC

To access this sign, one needs to look at the interference term introduced in Equation (82) which depends linearly on the CFF [149]. Even better, one can look at the beam spin asymmetry, selecting on the polarised part of the interference and defined as:

$$A_{LU} = \frac{d\sigma^\uparrow - d\sigma^\downarrow}{d\sigma^\uparrow + d\sigma^\downarrow}. \tag{84}$$

At leading-twist, the latter is proportional to the imaginary part of the CFF $\mathcal{H}$. If gluons are strong enough to flip the sign of the polarised interference, it would trigger a flip in the sign of the asymmetry.

Two models were used to assess whether DVCS on a virtual pion would be possible, and if one would see a sign change in the beam spin asymmetry. The results are shown on Figure 14. The first model is a theoretically complete model built in ref. [58] and exploiting the state-of-th-art results on the pion PDF from Continuum Schwinger method techniques [118]. The second one is a phenomenological model, based on the Radyushkin Ansatz [55] and the GRS PDF [155]. The necessary evolution was performed by the Apfel++ software [92,94–96] interfaced with PARTONS [97]. The conclusions are clearly different from the contributions of the sole Bethe–Heitler process at typical EIC kinematics, allowing us to hope that DVCS on virtual pion will be measurable at this future facility. Moreover, the sign of the asymmetry is flipped, highlighting the strength of gluons, and this in both models. Thus, even if pion GPDs will not be extracted from experimental data, the latter will be able to assess the strength of gluons, and scan it with respect to Q^2, making an excellent physics case for the measurement of the Sullivan process at EIC.

In the case of EicC, since the kinematics probe the valence region, one is less sensitive to gluons. Nevertheless, the destructive interferences of quark and gluon trigger a sizeable reduction of the amplitude of the asymmetry, and make it sensitive to the Q^2 value probed [148]. This is also a valuable piece of experimental information that could be delivered in the future regarding pion GPDs.
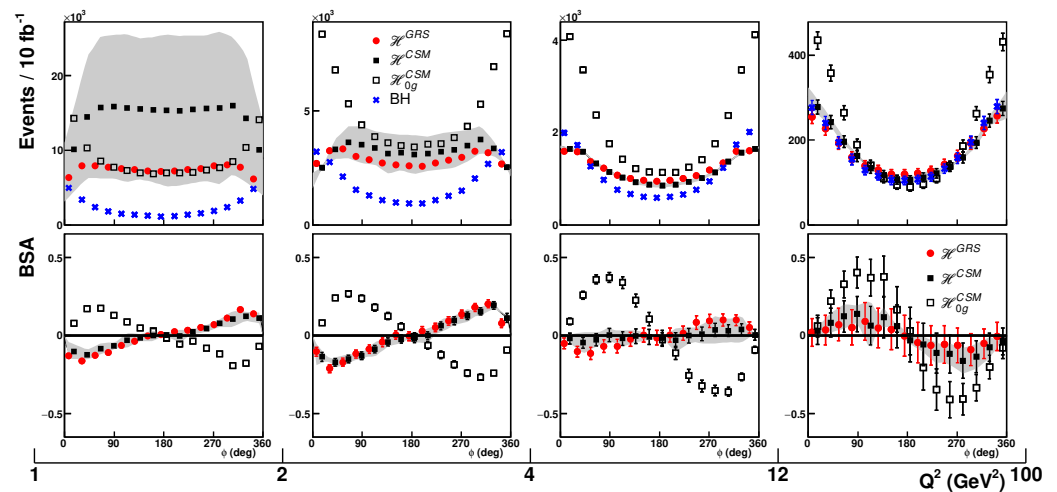
Figure 14. Upper band: number of events assessed as a function of ϕ for different bin in Q^2. The blue crosses correspond to the Bethe–Heitler signal only, the black square—to the theoretically complete model of ref. [58] with a CSM-based forward limit. The open square correspond to the same model but with gluons set to zero in the CFF. The red circles correspond to a phenomenological model with the GRS PDF [155] as an input for the forward limit. The grey band corresponds to the uncertainty of the CSM model associated with the choice of the initial evolution scale. Lower band: associated beam spin asymmetries. The sign flip is visible with the model from ref. [58]. Figure from ref. [148].

3.5. Challenges

The procedure described above and the very encouraging results which have been obtained might make one thing that the problem of computing GPDs for mesons is solved. However, some challenges remain that we will highlight in this section.

3.5.1. The Wilson Line

The first difficulty comes with the Wilson line $\mathcal{W}$ introduced in Equation (8). When we discussed the properties of the GPDs, we assumed that we were working in the lightcone gauge, where $\mathcal{W}$ is reduced to 1. However, in practice, the Bethe–Salpeter equation is mostly solved in the Landau gauge. There are two main reasons for this: the Landau gauge is the one used for fixed-gauge lattice QCD computation, allowing to compare N-point functions computed from lattice and continuum methods, and because the Landau gauge is a fixed point of the renormalisation group equation, and thus the gauge parameter does not run. Therefore, a fully consistent computation of the GPDs would require computing also the contribution of the Wilson line.

One of the possibility to bypass this problem would be to solve the Bethe–Salpeter and Dyson–Schwinger equations in the lightcone gauge. It is one of the clearest ways to provide a fully consistent description of GPDs through the overlap of LFWFs, avoiding gauge-related difficulties. As we mentioned before, this would trigger additional complications when solving the Dyson–Schwinger and Bethe–Salpeter equations, but remain feasible [156]. However, it would require a significant amount of work as all modern computations would need to be re-adapted for this specific gauge, without any lattice-QCD guidance.

In the case of the impulse approximation, attempts to describe the Wilson line perturbatively have been pursued (see [157]). However, because of the limitations of the impulse approximation already mentioned before, it is unclear that such a procedure could be generalised beyond the NJL model employed there.

3.5.2. Non-Perturbative Renormalisation

Another difficulty lies in the renormalisation properties of the operator already discussed before. One would expect that a two-body description would be valid only at low scale of QCD, a region which cannot be described using standard perturbative QCD. Yet,

the renormalisation properties of the twist-two operators are known only perturbatively, generating questions on whether one could use perturbative evolution equations at low scales. Models and prescriptions have been introduced, relying on a saturating coupling in the infrared (see, e.g., [158,159]). However, it is in principle possible to really derive non-perturbative renormalisation group equations for the twist two operators, consistently with the way the Dyson–Schwinger and Bethe–Salpeter equation are renormalised. A way to proceed here would be to look at the local twist-two operators and compute their associated renormalisation constants. However, one would expect that such a procedure would be feasible only for the lowest ones, as in the Landau gauge, the number of gluon fields entering the definition of the operator increases linearly with the order of the operator itself. Nevertheless, renormalising non-perturbatively the lowest-order twist-two operators would already provide insights on the size of the uncertainties associated with perturbative evolution at low scale.

Finally, let us add that for phenomenology purposes, one would need to manipulate objects renormalised in a consistent way, i.e., using the same renormalisation scheme. As most coefficient functions are computed in the $\overline{\text{MS}}$ scheme, it is, in principle, necessary to match the non-perturbative scheme to $\overline{\text{MS}}$, at a given order of perturbation theory. Since, for the moment, only perturbative evolution is used (though in an improved for with a saturating coupling), this question has not been treated in the continuum literature but will be brought to light once a non-perturbative renormalisation strategy is put in place.

3.5.3. The *D*-Term

Through the modelling procedure, we have also highlighted a difficulty regarding our ability to extract the so-called *D*-term when extending GPDs from the DGLAP to ERBL regions. Indeed, the *D*-term appears as a singularity on the $\beta = 0$ line (see Equation (44)), which remains ambiguous through the covariant extension technique presented here. The soft pion theorem of Equations (17) and (18) provides an anchor for vanishing t in the chiral limit. Moreover, the large t behaviour is known in perturbative QCD [160]. Yet in between, one is left with a hole to fill through modelling, in the absence of better treatment of this specific contribution. It was shown in ref. [135] that the question of the determination of the D-term was equivalent to the assumption of the J = 0 fixed pole in the Regge theory of Compton Scattering and that, for the moment, there is no other way than measuring specific sum rules connected to the *D*-term in order to tame the ambiguity on the latter.

4. From Mesons to Baryons

Having discussed in detail the results obtained regarding meson GPDs, we provide here some hints at how this can be generalised to baryons, as pioneering studies are still ongoing [161].

4.1. Nucleon LFWFs

The first complication between the pion and the nucleon, is that the lower Fock state of the latter is made of three quarks instead of two. This obviously increases the number of degrees of freedom and thus complicates the computation of three-body Bethe–Salpeter equation (also called the Faddeev equation). Techniques to compute the latter relying either on a quark–diquark picture (see, e.g., [162–164]) or using a three-quark picture [165–167] have been developed. Consequently, it is in principle possible to follow the mesons' path and project the solution of these covariant equations onto the lightfront. The expected result is composed of six independent lightfront wave functions (see [168]) characterising the possible three quarks fluctuations of the nucleon and carrying a given amount of orbital angular momentum.

A first attempt of computing the LFWFs in such a formalism has been pursued in the quark-diquark picture and led to computation of the leading-twist distribution amplitude [169,170]. The computations have highlighted several interesting points. First, it validated the extension of the meson framework toward the baryon ones. Then, it showed

that the quark–diquark computations yield very similar results with respect to the lattice QCD simulations of the first Mellin moments, highlighting that this kind of approximation is indeed valuable, as explained in great details in ref. [171]. Finally, a third point of interest is the noticeable difference between the Distribution Amplitude of the nucleon and the Roper resonance highlighted in ref. [169]. Indeed, while the distribution amplitude of the nucleon is positive definite, the one of the Roper resonance changes sign, meaning there is a kinematic area which is forbidden. This behaviour is similar to what one expects in non-relativistic quantum mechanics regarding higher excited states. One may thus expect significant differences between the nucleon GPDs and resonances GPD from such a comparison of Distribution amplitude. We expect that these differences also impact the 1+2D probability densities to find quarks and gluons at a given position of the transverse plane, reinforcing the interest in the computation of excited states GPDs.

4.2. Nucleon GPDs

Once the nucleon LFWFs are at hand, the formalism of overlap of LFWFs can be applied in the same way as for the pion, with some small differences. The first one is that because nucleons are spin 1/2 particles, one needs several GPDs to parametrise the considered leading twist matrix element (see Equation (9)). As a result, the overlap representation will naively yield combinations of GPDs. The latter can be disentangled by playing with the incoming and outgoing nucleon helicity projections (see, for instance, [84]). Multiple GPDs, means multiple DDs to extract as, in the case of the nucleon, Equation (44) is modified to:

$$H(x,\xi,t) = \int_\Omega \mathrm{d}\beta\mathrm{d}\alpha\,\delta(x-\beta-\alpha\xi)[F(\beta,\alpha,t)+\xi\delta(\beta)D(\alpha,t)], \tag{85}$$

$$E(x,\xi,t) = \int_\Omega \mathrm{d}\beta\mathrm{d}\alpha\,\delta(x-\beta-\alpha\xi)[K(\beta,\alpha,t)-\xi\delta(\beta)D(\alpha,t)]. \tag{86}$$

Consequently, two DDs, *F* and *K*, need to be extracted following the covariant extension procedure. Rather than extracting them independently, it may be better to focus on $H+E$, which is directly a "true" Radon transform, without an additional *D*-term, and $-E$, as it was suggested in ref. [39,172] and put in practice in phenomenological extractions in ref. [57]. The stability of the incomplete inverse Radon transform remains to be assessed in the case of the nucleon.

This decomposition allows us to highlight that the issue of the *D*-term is more difficult to handle in the case of the nucleon, with respect to the pion. Indeed, to the best of our knowledge, there is no equivalent in the nucleon case of the soft pion theorem, and thus, a theoretical constrain providing us with information on the *D*-term is lost. If the large-*t* expansion in perturbative QCD has been computed (see ref. [160]), at experimentally achievable values of *t* (and small enough so that collinear factorisation works), there is for the moment no theoretical guidance on the value of this function. It is noticeable though that, at the time of writing, phenomenological extractions of the nucleon *D*-term based on the DVCS dispersion relations (see [173,174]) provide results which remain compatible with zero [71,175]. This situation might change with the more precise DVCS data provided by the upgraded facilities of the Jefferson Laboratory [19,20].

With the expected wealth of new experimental data coming from Jefferson Laboratory in the following years, the question of a consistent description of experimental data using GPDs computed with continuum technique has never been more relevant. The impact of the Wilson line together with that of non-perturbative renormalisation are expected to be at the core of future theoretical developments. Finally, let us highlight that the overlap of LFWFs will also allow us to compute using continuum techniques the standard nucleon PDFs and the standard nucleon EFFs.

4.3. Transition GPDs

Beyond the nucleon GPDs, we would like to highlight that our formalism is able to handle all spin 1/2 baryons GPDs (providing that computations of the associated Faddeev wave function are available), but also transition GPDs, between two different baryons. Among all possible transitions, the better experimentally accessible one is certainly the nucleon-to-delta transition [176,177]. One can indeed define a transition DVCS process, such that $ep \rightarrow e\Delta^+\gamma$, which factorises between the standard DVCS hard coefficient function and nucleon-to-delta transition GPDs. Such a complementary channel provides an indirect way to probe the internal structure of the delta particle, as in the continuum framework, one would need to compute the transition GPDs as an overlap between the nucleon and delta LFWFs. This will allow to shed light on the delta LFWFs, and thus provide feedback on the solution of the Faddeev equations for baryons other than the nucleon. We expect that it provides guidance in our understanding of the three-body interaction and its consequences in QCD.

5. Conclusions

Concluding this review paper, we would like to highlight again that GPDs provide a unique way to map hadrons in 3D and gain experimental insights into their energy-momentum tensor. However, the path toward reliable models and computations of GPDs remains difficult. We have highlighted how using continuum techniques, one could manage to compute GPDs who fulfil all required theoretical constrains, and more specifically, both positivity and polynomiality. It relies on the projection of the solutions of the Bethe–Salpeter equations (or Faddeev equation for baryons) onto the lightfront, so that one obtains the so-called lightfront wave functions. GPDs can then be expressed as an overlap of lightfront wave functions in the so-called DGLAP region, ensuring the positivity is fulfilled. Then, they are extended to the ERBL region using the covariant extension, which guarantees the polynomiality property.

This technique has been successfully applied to mesons, and it has provided estimates of counting rates for DVCS on virtual pion through the Sullivan process, showing that one can expect such a process to be measurable. Regarding the nucleon, part of the path toward the building of a GPD model has been performed, but some of the work remain to be completed. Today, the baryon sector appears as the target to reach in the forthcoming years.

Abbreviations

The following abbreviations are used in this manuscript:

DDs	Double Distributions
DGLAP	Dokshitzer–Gribov–Lipatov–Altarelli–Parisi
DVCS	Deep Virtual Compton Scattering

EFFs	Electromagnetic Form Factors
EIC	Electron Ion Collider
EicC	Electron Ion collider in China
EMT	Energy Momentum Tensor
ERBL	Efremov–Radyushkin–Brodsky–Lepage
GPDs	Generalised Parton Distribution
GTMDs	Generalised Transverse Momentum dependent Distributions
JLab	Jefferson Laboratory
LFWFs	Lightfront Wave Functions
NJL	Nambu–Jona-Lasinio
PDFs	Parton Distribution Functions
QCD	Quantum Chromodynamics
RGE	Renormalisation Group Equation
TMDs	Transverse Momentum dependent Distributions

References

1. Bjorken, J. Asymptotic Sum Rules at Infinite Momentum. *Phys. Rev.* **1969**, *179*, 1547–1553. [CrossRef]
2. Altarelli, G.; Parisi, G. Asymptotic Freedom in Parton Language. *Nucl. Phys.* **1977**, *B126*, 298. [CrossRef]
3. Gribov, V.; Lipatov, L. Deep inelastic e p scattering in perturbation theory. *Sov. J. Nucl. Phys.* **1972**, *15*, 438–450.
4. Dokshitzer, Y.L. Calculation of the Structure Functions for Deep Inelastic Scattering and e+ e− Annihilation by Perturbation Theory in Quantum Chromodynamics. *Sov. Phys. JETP* **1977**, *46*, 641–653.
5. Ji, X.D. Gauge-Invariant Decomposition of Nucleon Spin. *Phys. Rev. Lett.* **1997**, *78*, 610–613. [CrossRef]
6. Mueller, D.; Robaschik, D.; Geyer, B.; Dittes, F.; Hořejši, J. Wave functions, evolution equations and evolution kernels from light ray operators of QCD. *Fortsch. Phys.* **1994**, *42*, 101–141. [CrossRef]
7. Radyushkin, A. Nonforward parton distributions. *Phys. Rev.* **1997**, *D56*, 5524–5557. [CrossRef]
8. Collins, J.C.; Soper, D.E.; Sterman, G.F. Transverse Momentum Distribution in Drell-Yan Pair and W and Z Boson Production. *Nucl. Phys. B* **1985**, *250*, 199–224. [CrossRef]
9. Collins, J. *Foundations of Perturbative QCD*; Cambridge University Press: Cambridge, UK, 2013; Volume 32.
10. Burkardt, M. Impact parameter dependent parton distributions and off forward parton distributions for zeta —> 0. *Phys. Rev.* **2000**, *D62*, 071503; Erratum in *Phys. Rev.* **2002**, *D66*, 119903. [CrossRef]
11. Diehl, M. Generalized parton distributions in impact parameter space. *Eur. Phys. J.* **2002**, *C25*, 223–232. [CrossRef]
12. Ji, X.d. Viewing the proton through 'color' filters. *Phys. Rev. Lett.* **2003**, *91*, 062001. [CrossRef] [PubMed]
13. Belitsky, A.V.; Ji, X.d.; Yuan, F. Quark imaging in the proton via quantum phase space distributions. *Phys. Rev.* **2004**, *D69*, 074014. [CrossRef]
14. Meissner, S.; Metz, A.; Schlegel, M. Generalized parton correlation functions for a spin-1/2 hadron. *J. High Energy Phys.* **2009**, *0908*, 056. [CrossRef]
15. Meissner, S.; Metz, A.; Schlegel, M.; Goeke, K. Generalized parton correlation functions for a spin-0 hadron. *J. High Energy Phys.* **2008**, *0808*, 038. [CrossRef]
16. Lorce, C.; Pasquini, B. Quark Wigner Distributions and Orbital Angular Momentum. *Phys. Rev.* **2011**, *D84*, 014015. [CrossRef]
17. Echevarria, M.G.; Idilbi, A.; Kanazawa, K.; Lorcé, C.; Metz, A.; Pasquini, B.; Schlegel, M. Proper definition and evolution of generalized transverse momentum dependent distributions. *Phys. Lett. B* **2016**, *759*, 336–341. [CrossRef]
18. Hatta, Y.; Xiao, B.W.; Yuan, F. Probing the Small- x Gluon Tomography in Correlated Hard Diffractive Dijet Production in Deep Inelastic Scattering. *Phys. Rev. Lett.* **2016**, *116*, 202301. [CrossRef] [PubMed]
19. Georges, F.; Rashad, M.N.H.; Stefanko, A.; Dlamini, M.; Karki, B.; Ali, S.F.; Lin, P.; Ko, H.; Israel, N.; Adikaram, D.; et al. Deeply Virtual Compton Scattering Cross Section at High Bjorken xB. *Phys. Rev. Lett.* **2022**, *128*, 252002. [CrossRef]
20. Christiaens, G.; Defurne, M.; Sokhan, D.; Achenbach, P.; Akbar, Z.; Amaryan, M.J.; Atac, H.; Avakian, H.; Gayoso, C.A.; Baashen, L.; et al. First CLAS12 measurement of DVCS beam-spin asymmetries in the extended valence region. *arXiv* **2022**, arXiv:2211.11274.
21. Catani, S.; de Florian, D.; Grazzini, M. Universality of nonleading logarithmic contributions in transverse momentum distributions. *Nucl. Phys. B* **2001**, *596*, 299–312. [CrossRef]
22. Echevarria, M.G.; Scimemi, I.; Vladimirov, A. Unpolarized Transverse Momentum Dependent Parton Distribution and Fragmentation Functions at next-to-next-to-leading order. *J. High Energy Phys.* **2016**, *2016*, 4. [CrossRef]

23. Bertone, V. Matching generalised transverse-momentum-dependent distributions onto generalised parton distributions at one loop. *Eur. Phys. J. C* **2022**, *82*, 941. [CrossRef]

24. Braun, V.; Müller, D. Exclusive processes in position space and the pion distribution amplitude. *Eur. Phys. J. C* **2008**, *55*, 349–361. [CrossRef]

25. Ji, X. Parton Physics on a Euclidean Lattice. *Phys. Rev. Lett.* **2013**, *110*, 262002. [CrossRef]

26. Radyushkin, A.V. Quasi-parton distribution functions, momentum distributions, and pseudo-parton distribution functions. *Phys. Rev. D* **2017**, *96*, 034025. [CrossRef]

27. Alexandrou, C.; Cichy, K.; Constantinou, M.; Jansen, K.; Scapellato, A.; Steffens, F. Light-Cone Parton Distribution Functions from Lattice QCD. *Phys. Rev. Lett.* **2018**, *121*, 112001. [CrossRef]

28. Egerer, C.; Edwards, R.G.; Kallidonis, C.; Orginos, K.; Radyushkin, A.V.; Richards, D.G.; Romero, E.; Zafeiropoulos, S. Towards high-precision parton distributions from lattice QCD via distillation. *J. High Energy Phys.* **2021**, *11*, 148. [CrossRef]

29. Constantinou, M.; Courtoy, A.; Ebert, M.A.; Engelhardt, M.; Giani, T.; Hobbs, T.; Hou, T.-J.; Kusina, A.; Kutak, K.; Liang, J.; et al. Parton distributions and lattice-QCD calculations: Toward 3D structure. *Prog. Part. Nucl. Phys.* **2021**, *121*, 103908. [CrossRef]

30. Nakanishi, N. A General survey of the theory of the Bethe-Salpeter equation. *Prog. Theor. Phys. Suppl.* **1969**, *43*, 1–81. [CrossRef]

31. Nakanishi, N. *Graph Theory and Feynman Integrals*; Gordon and Breach: New York, NY, USA, 1971.

32. Binosi, D.; Tripolt, R.A. Spectral functions of confined particles. *Phys. Lett. B* **2020**, *801*, 135171, [CrossRef]

33. Eichmann, G.; Ferreira, E.; Stadler, A. Going to the light front with contour deformations. *Phys. Rev. D* **2022**, *105*, 034009. [CrossRef]

34. Aguilar, A.C.; Cardona, J.C.; Ferreira, M.N.; Papavassiliou, J. Non-Abelian Ball-Chiu vertex for arbitrary Euclidean momenta. *Phys. Rev.* **2017**, *D96*, 014029. [CrossRef]

35. Aguilar, A.C.; Ferreira, M.N.; Figueiredo, C.T.; Papavassiliou, J. Nonperturbative Ball-Chiu construction of the three-gluon vertex. *Phys. Rev. D* **2019**, *99*, 094010. [CrossRef]

36. Aguilar, A.C.; De Soto, F.; Ferreira, M.N.; Papavassiliou, J.; Rodríguez-Quintero, J.; Zafeiropoulos, S. Gluon propagator and three-gluon vertex with dynamical quarks. *Eur. Phys. J. C* **2020**, *80*, 154. [CrossRef]

37. Aguilar, A.C.; Ferreira, M.N.; Papavassiliou, J. Exploring smoking-gun signals of the Schwinger mechanism in QCD. *Phys. Rev. D* **2022**, *105*, 014030. [CrossRef]

38. Diehl, M. Generalized parton distributions. *Phys. Rep.* **2003**, *388*, 41–277. [CrossRef]

39. Belitsky, A.; Radyushkin, A. Unraveling hadron structure with generalized parton distributions. *Phys. Rep.* **2005**, *418*, 1–387. [CrossRef]

40. Kumericki, K.; Liuti, S.; Moutarde, H. GPD phenomenology and DVCS fitting. *Eur. Phys. J.* **2016**, *A52*, 157. [CrossRef]

41. Mezrag, C. An Introductory Lecture on Generalised Parton Distributions. *Few Body Syst.* **2022**, *63*, 62. [CrossRef]

42. Mezrag, C.; Moutarde, H.; Rodriguez-Quintero, J. From Bethe–Salpeter Wave functions to Generalised Parton Distributions. *Few Body Syst.* **2016**, *57*, 729–772. [CrossRef]

43. Ji, X.D. Deeply virtual Compton scattering. *Phys. Rev.* **1997**, *D55*, 7114–7125. [CrossRef]

44. Radyushkin, A. Asymmetric gluon distributions and hard diffractive electroproduction. *Phys. Lett.* **1996**, *B385*, 333–342. [CrossRef]

45. Diehl, M.; Gousset, T.; Pire, B.; Teryaev, O. Probing partonic structure in gamma* gamma —> pi pi near threshold. *Phys. Rev. Lett.* **1998**, *81*, 1782–1785. [CrossRef]

46. Polyakov, M.V. Hard exclusive electroproduction of two pions and their resonances. *Nucl. Phys.* **1999**, *B555*, 231. [CrossRef]

47. Kivel, N.; Mankiewicz, L.; Polyakov, M.V. NLO corrections and contribution of a tensor gluon operator to the process gamma* gamma —> pi pi. *Phys. Lett. B* **1999**, *467*, 263–270. [CrossRef]

48. Diehl, M.; Gousset, T.; Pire, B. Exclusive production of pion pairs in gamma* gamma collisions at large Q**2. *Phys. Rev.* **2000**, *D62*, 073014. [CrossRef]

49. Diehl, M.; Gousset, T. Time ordering in off diagonal parton distributions. *Phys. Lett.* **1998**, *B428*, 359–370. [CrossRef]

50. Efremov, A.; Radyushkin, A. Asymptotical Behavior of Pion Electromagnetic Form-Factor in QCD. *Theor. Math. Phys.* **1980**, *42*, 97–110.[CrossRef]

51. Efremov, A.; Radyushkin, A. Factorization and Asymptotical Behavior of Pion Form-Factor in QCD. *Phys. Lett.* **1980**, *B94*, 245–250. [CrossRef]

52. Lepage, G.P.; Brodsky, S.J. Exclusive Processes in Quantum Chromodynamics: Evolution Equations for Hadronic Wave Functions and the Form-Factors of Mesons. *Phys. Lett.* **1979**, *B87*, 359–365. [CrossRef]

53. Lepage, G.P.; Brodsky, S.J. Exclusive Processes in Perturbative Quantum Chromodynamics. *Phys. Rev.* **1980**, *D22*, 2157. [CrossRef]

54. Vanderhaeghen, M.; Guichon, P.A.; Guidal, M. Deeply virtual electroproduction of photons and mesons on the nucleon: Leading order amplitudes and power corrections. *Phys. Rev.* **1999**, *D60*, 094017. [CrossRef]
55. Musatov, I.; Radyushkin, A. Evolution and models for skewed parton distributions. *Phys. Rev.* **2000**, *D61*, 074027. [CrossRef]
56. Goloskokov, S.; Kroll, P. Vector meson electroproduction at small Bjorken-x and generalized parton distributions. *Eur. Phys. J.* **2005**, *C42*, 281–301. [CrossRef]
57. Mezrag, C.; Moutarde, H.; Sabatié, F. Test of two new parameterizations of the Generalized Parton Distribution *H*. *Phys. Rev.* **2013**, *D88*, 014001. [CrossRef]
58. Chavez, J.M.M.; Bertone, V.; De Soto Borrero, F.; Defurne, M.; Mezrag, C.; Moutarde, H.; Rodríguez-Quintero, J.; Segovia, J. Pion generalized parton distributions: A path toward phenomenology. *Phys. Rev. D* **2022**, *105*, 094012. [CrossRef]
59. Raya, K.; Cui, Z.F.; Chang, L.; Morgado, J.M.; Roberts, C.D.; Rodriguez-Quintero, J. Revealing pion and kaon structure via generalised parton distributions. *Chin. Phys. C* **2022**, *46*, 013105. [CrossRef]
60. Mezrag, C.; Chang, L.; Moutarde, H.; Roberts, C.D.; Rodríguez-Quintero, J.; Sabatié, F.; Schmidt, S.M. Sketching the pion's valence-quark generalised parton distribution. *Phys. Lett.* **2014**, *B741*, 190–196. [CrossRef]
61. Moutarde, H.; Sznajder, P.; Wagner, J. Border and skewness functions from a leading order fit to DVCS data. *Eur. Phys. J.* **2018**, *C78*, 890. [CrossRef]
62. Khalek, R.A.; Accardi, A.; Adam, J.; Adamiak, D.; Akers, W.; Albaladejo, M.; Al-bataineh, A.; Alexeev, M.G.; Ameli, F.; Antonioli, P.; et al. Science Requirements and Detector Concepts for the Electron-Ion Collider: EIC Yellow Report. *arXiv* **2021**, arXiv:2103.05419.
63. Anderle, D.P.; Bertone, V.; Cao, X.; Chang, L.; Chang, N.; Chen, G.; Chen, X.; Chen, Z.; Cui, Z.; Dai, L.; et al. Electron-ion collider in China. *Front. Phys.* **2021**, *16*, 64701. [CrossRef]
64. Polyakov, M.V.; Schweitzer, P. Forces inside hadrons: pressure, surface tension, mechanical radius, and all that. *Int. J. Mod. Phys. A* **2018**, *33*, 1830025. [CrossRef]
65. Bakker, B.L.G.; Leader, E.; Trueman, T.L. A Critique of the angular momentum sum rules and a new angular momentum sum rule. *Phys. Rev. D* **2004**, *70*, 114001. [CrossRef]
66. Leader, E.; Lorcé, C. The angular momentum controversy: What's it all about and does it matter? *Phys. Rep.* **2014**, *541*, 163–248. [CrossRef]
67. Brodsky, S.J.; Hwang, D.S.; Ma, B.Q.; Schmidt, I. Light cone representation of the spin and orbital angular momentum of relativistic composite systems. *Nucl. Phys. B* **2001**, *593*, 311–335. [CrossRef]
68. Lowdon, P.; Chiu, K.Y.J.; Brodsky, S.J. Rigorous constraints on the matrix elements of the energy-momentum tensor. *Phys. Lett. B* **2017**, *774*, 1–6. [CrossRef]
69. Lorcé, C.; Lowdon, P. Universality of the Poincaré gravitational form factor constraints. *Eur. Phys. J. C* **2020**, *80*, 207. [CrossRef]
70. Lorcé, C.; Mantovani, L.; Pasquini, B. Spatial distribution of angular momentum inside the nucleon. *Phys. Lett. B* **2018**, *776*, 38–47. [CrossRef]
71. Dutrieux, H.; Lorcé, C.; Moutarde, H.; Sznajder, P.; Trawiński, A.; Wagner, J. Phenomenological assessment of proton mechanical properties from deeply virtual Compton scattering. *Eur. Phys. J. C* **2021**, *81*, 300, . [CrossRef]
72. Polyakov, M.V. Generalized parton distributions and strong forces inside nucleons and nuclei. *Phys. Lett.* **2003**, *B555*, 57–62. [CrossRef]
73. Lorcé, C.; Moutarde, H.; Trawiński, A.P. Revisiting the mechanical properties of the nucleon. *Eur. Phys. J. C* **2019**, *79*, 89. [CrossRef]
74. Ji, X.D. Off forward parton distributions. *J. Phys.* **1998**, *G24*, 1181–1205. [CrossRef]
75. Radyushkin, A. Symmetries and structure of skewed and double distributions. *Phys. Lett.* **1999**, *B449*, 81–88. [CrossRef]
76. Hausdorff, F. Summationsmethoden und Momentfolgen. I. *Math. Z.* **1921**, *9*, 74–109. [CrossRef]
77. Hausdorff, F. Summationsmethoden und Momentfolgen. II. *Math. Z.* **1921**, *9*, 280–299. [CrossRef]
78. Hertle, A. Continuity of the Radon transform and its inverse on euclidean space. *Math. Z.* **1983**, *184*, 165–192. [CrossRef]
79. Radon, J. Über die Bestimmung von Funktionen durch ihre Integralwerte längs gewisser Mannigfaltigkeiten. *Akad. Wiss.* **1917**, *69*, 262.
80. Radon, J. On the determination of functions from their integral values along certain manifolds. *IEEE Trans. Med. Imaging* **1986**, *5*, 170–176. [CrossRef]
81. Polyakov, M.V.; Weiss, C. Skewed and double distributions in pion and nucleon. *Phys. Rev.* **1999**, *D60*, 114017. [CrossRef]
82. Teryaev, O. Crossing and radon tomography for generalized parton distributions. *Phys. Lett.* **2001**, *B510*, 125–132. [CrossRef]
83. Chouika, N.; Mezrag, C.; Moutarde, H.; Rodríguez-Quintero, J. Covariant Extension of the GPD overlap representation at low Fock states. *Eur. Phys. J.* **2017**, *C77*, 906. [CrossRef]
84. Diehl, M.; Feldmann, T.; Jakob, R.; Kroll, P. The Overlap representation of skewed quark and gluon distributions. *Nucl. Phys.* **2001**, *B596*, 33–65. [CrossRef]

85. Chouika, N.; Mezrag, C.; Moutarde, H.; Rodríguez-Quintero, J. A Nakanishi-based model illustrating the covariant extension of the pion GPD overlap representation and its ambiguities. *Phys. Lett.* **2018**, *B780*, 287–293. [CrossRef]

86. Rinaldi, M. GPDs at non-zero skewness in ADS/QCD model. *Phys. Lett. B* **2017**, *771*, 563–567. [CrossRef]

87. Shi, C.; Bednar, K.; Cloët, I.C.; Freese, A. Spatial and Momentum Imaging of the Pion and Kaon. *Phys. Rev. D* **2020**, *101*, 074014. [CrossRef]

88. Radyushkin, A. Double distributions and evolution equations. *Phys. Rev.* **1999**, *D59*, 014030, [CrossRef]

89. Pire, B.; Soffer, J.; Teryaev, O. Positivity constraints for off-forward parton distributions. *Eur. Phys. J.* **1999**, *C8*, 103–106. [CrossRef]

90. Pobylitsa, P. Disentangling positivity constraints for generalized parton distributions. *Phys. Rev.* **2002**, *D65*, 114015. [CrossRef]

91. Pobylitsa, P. Inequalities for generalized parton distributions H and E. *Phys. Rev.* **2002**, *D65*, 077504, [CrossRef]

92. Bertone, V.; Dutrieux, H.; Mezrag, C.; Morgado, J.M.; Moutarde, H. Revisiting evolution equations for generalised parton distributions. *Eur. Phys. J. C* **2022**, *82*, 888. [CrossRef]

93. Vinnikov, A. Code for prompt numerical computation of the leading order GPD evolution. *arXiv* **2006**, arXiv:hep-ph/hep-ph/0604248.

94. Bertone, V.; Carrazza, S.; Rojo, J. APFEL: A PDF Evolution Library with QED corrections. *Comput. Phys. Commun.* **2014**, *185*, 1647–1668. [CrossRef]

95. Bertone, V.; Carrazza, S.; Hartland, N.P. APFELgrid: a high performance tool for parton density determinations. *Comput. Phys. Commun.* **2017**, *212*, 205–209. [CrossRef]

96. Bertone, V. APFEL++: A new PDF evolution library in C++. *PoS* **2018**, *DIS2017*, 201. [CrossRef]

97. Berthou, B.; Binosi, D.; Chouika, N.; Colaneri, L.; Guidal, M.; Mezrag, C.; Moutarde, H.; Rodríguez-Quintero, J.; Sabatié, F.; Sznajder, P.; et al. PARTONS: PARtonic Tomography Of Nucleon Software. A computing framework for the phenomenology of Generalized Parton Distributions. *Eur. Phys. J.* **2018**, *C78*, 478. [CrossRef]

98. Ohrndorf, T. Constraints From Conformal Covariance on the Mixing of Operators of Lowest Twist. *Nucl. Phys. B* **1982**, *198*, 26–44. [CrossRef]

99. Mueller, D.; Schafer, A. Complex conformal spin partial wave expansion of generalized parton distributions and distribution amplitudes. *Nucl. Phys.* **2006**, *B739*, 1–59. [CrossRef]

100. Kumericki, K.; Mueller, D.; Passek-Kumericki, K. Towards a fitting procedure for deeply virtual Compton scattering at next-to-leading order and beyond. *Nucl. Phys. B* **2008**, *794*, 244–323. [CrossRef]

101. Müller, D.; Lautenschlager, T.; Passek-Kumericki, K.; Schaefer, A. Towards a fitting procedure to deeply virtual meson production—The next-to-leading order case. *Nucl. Phys.* **2014**, *B884*, 438–546. [CrossRef]

102. Belitsky, A.V.; Mueller, D. Next-to-leading order evolution of twist-2 conformal operators: The Abelian case. *Nucl. Phys.* **1998**, *B527*, 207–234. [CrossRef]

103. Belitsky, A.V.; Mueller, D. Exclusive evolution kernels in two loop order: Parity even sector. *Phys. Lett.* **1999**, *B464*, 249–256. [CrossRef]

104. Belitsky, A.V.; Mueller, D.; Freund, A. Reconstruction of nonforward evolution kernels. *Phys. Lett.* **1999**, *B461*, 270–279. [CrossRef]

105. Belitsky, A.V.; Freund, A.; Mueller, D. Evolution kernels of skewed parton distributions: Method and two loop results. *Nucl. Phys.* **2000**, *B574*, 347–406. [CrossRef]

106. Braun, V.M.; Manashov, A.N.; Moch, S.; Strohmaier, M. Two-loop evolution equations for flavor-singlet light-ray operators. *J. High Energy Phys.* **2019**, *02*, 191. [CrossRef]

107. Braun, V.M.; Manashov, A.N.; Moch, S.; Strohmaier, M. Three-loop evolution equation for flavor-nonsinglet operators in off-forward kinematics. *J. High Energy Phys.* **2017**, *06*, 037. [CrossRef]

108. Mueller, D. The Evolution of the pion distribution amplitude in next-to-leading-order. *Phys. Rev.* **1995**, *D51*, 3855–3864. [CrossRef]

109. Braun, V.M.; Manashov, A.N.; Moch, S.; Schoenleber, J. Two-loop coefficient function for DVCS: vector contributions. *J. High Energy Phys.* **2020**, *09*, 117. [CrossRef]

110. Pobylitsa, P.V. Integral representations for nonperturbative GPDs in terms of perturbative diagrams. *Phys. Rev. D* **2003**, *67*, 094012. [CrossRef]

111. Theussl, L.; Noguera, S.; Vento, V. Generalized parton distributions of the pion in a Bethe-Salpeter approach. *Eur. Phys. J.* **2004**, *A20*, 483–498. [CrossRef]

112. Tiburzi, B.; Miller, G. Generalized parton distributions and double distributions for q anti-q pions. *Phys. Rev.* **2003**, *D67*, 113004. [CrossRef]

113. Mezrag, C.; Moutarde, H.; Rodríguez-Quintero, J.; Sabatié, F. Towards a Pion Generalized Parton Distribution Model from Dyson-Schwinger Equations. *arXiv* **2014**, arXiv:1406.7425.

114. Chang, L.; Mezrag, C.; Moutarde, H.; Roberts, C.D.; Rodriguez-Quintero, J.; Tandy, P.C. Basic features of the pion valence-quark distribution function. *Phys. Lett.* **2014**, *B737*, 23–29. [CrossRef]

115. Binosi, D.; Chang, L.; Papavassiliou, J.; Qin, S.X.; Roberts, C.D. Symmetry preserving truncations of the gap and Bethe-Salpeter equations. *Phys. Rev. D* **2016**, *93*, 096010. [CrossRef]

116. Qin, S.X.; Roberts, C.D. Resolving the Bethe–Salpeter Kernel. *Chin. Phys. Lett.* **2021**, *38*, 071201. [CrossRef]

117. Nguyen, T.; Bashir, A.; Roberts, C.D.; Tandy, P.C. Pion and kaon valence-quark parton distribution functions. *Phys. Rev.* **2011**, *C83*, 062201. [CrossRef]

118. Ding, M.; Raya, K.; Binosi, D.; Chang, L.; Roberts, C.D.; Schmidt, S.M. Symmetry, symmetry breaking, and pion parton distributions. *Phys. Rev. D* **2020**, *101*, 054014. [CrossRef]

119. Broniowski, W.; Ruiz Arriola, E.; Golec-Biernat, K. Generalized parton distributions of the pion in chiral quark models and their QCD evolution. *Phys. Rev.* **2008**, *D77*, 034023. [CrossRef]

120. Freese, A.; Cloët, I.C. Impact of dynamical chiral symmetry breaking and dynamical diquark correlations on proton generalized parton distributions. *Phys. Rev. C* **2020**, *101*, 035203. [CrossRef]

121. Freese, A.; Cloët, I.C. Quark spin and orbital angular momentum from proton generalized parton distributions. *Phys. Rev. C* **2021**, *103*, 045204. [CrossRef]

122. Zhang, J.L.; Cui, Z.F.; Ping, J.; Roberts, C.D. Contact interaction analysis of pion GTMDs. *Eur. Phys. J. C* **2021**, *81*, 6 . [CrossRef]

123. Xing, Z.; Ding, M.; Raya, K.; Chang, L. A fresh look at the generalized parton distributions of light pseudoscalar mesons. *arXiv* **2023**, arXiv:2301.02958.

124. Lan, J.; Mondal, C.; Jia, S.; Zhao, X.; Vary, J.P. Pion and kaon parton distribution functions from basis light front quantization and QCD evolution. *Phys. Rev. D* **2020**, *101*, 034024. [CrossRef]

125. de Teramond, G.F.; Liu, T.; Sufian, R.S.; Dosch, H.G.; Brodsky, S.J.; Deur, A. Universality of Generalized Parton Distributions in Light-Front Holographic QCD. *Phys. Rev. Lett.* **2018**, *120*, 182001. [CrossRef]

126. Burkardt, M.; Ji, X.d.; Yuan, F. Scale dependence of hadronic wave functions and parton densities. *Phys. Lett.* **2002**, *B545*, 345–351. [CrossRef]

127. Chang, L.; Cloet, I.; Cobos-Martinez, J.; Roberts, C.; Schmidt, S.; Tandy, P.C. Imaging dynamical chiral symmetry breaking: pion wave function on the light front. *Phys. Rev. Lett.* **2013**, *110*, 132001. [CrossRef] [PubMed]

128. Xu, S.S.; Chang, L.; Roberts, C.D.; Zong, H.S. Pion and kaon valence-quark parton quasidistributions. *Phys. Rev. D* **2018**, *97*, 094014. [CrossRef]

129. Albino, L.; Higuera-Angulo, I.M.; Raya, K.; Bashir, A. Pseudoscalar mesons: Light front wave functions, GPDs, and PDFs. *Phys. Rev. D* **2022**, *106*, 034003. [CrossRef]

130. Mezrag, C.; Salmé, G. Fermion and Photon gap-equations in Minkowski space within the Nakanishi Integral Representation method. *Eur. Phys. J. C* **2021**, *81*, 34. [CrossRef]

131. Hwang, D.; Mueller, D. Implication of the overlap representation for modelling generalized parton distributions. *Phys. Lett.* **2008**, *B660*, 350–359. [CrossRef]

132. Müller, D. Double distributions and generalized parton distributions from the parton number conserved light front wave function overlap representation. *arXiv* **2017**, arXiv:1711.09932.

133. Boman, J.; Quinto, E.T. Support theorems for real-analytic Radon transforms. *Duke Math. J.* **1987**, *55*, 943–948. [CrossRef]

134. Chavez, J.M.M.; Dall'Olio P. ; De Soto Borrero, F. ; Mezrag, C. ; Moutarde, H. ; Rodriguez Quintero, J. ; Sznajder, P. ; Segovia, J. Reconstruction of Double distributions from limited GPD knowledge. 2023, *in preparation*.

135. Müller, D.; Semenov-Tian-Shansky, K.M. $J = 0$ fixed pole and D-term form factor in deeply virtual Compton scattering. *Phys. Rev.* **2015**, *D92*, 074025. [CrossRef]

136. Hadamard, J. Sur les problèmes aux dérivées partielles et leur signification physique. *Princet. Univ. Bull.* **1902**, *13*, 49–52.

137. Maz'ya, V.; Shaposhnikova, T. *Jacques Hadamard, a Universal Mathematician. History of Mathematics 14*; American Mathematical Society: Providence, RI, USA, 1998.

138. Natterer, F. *The Mathematics of Computerized Tomography*; Classics in Applied Mathematics; Society for Industrial and Applied Mathematics: Philadelphia, PA, USA, 2001.

139. Fong, D.; Saunders, M. LSMR: An iterative algorithm for sparse least-squares problems. *arXiv* **2010**, arXiv:1006.0758.

140. Press, W.H.; Flannery, B.P.; Teukolsky, S.A.; Vetterling, W.T. *Numerical Recipes*; Cambridge University Press: Cambridge, UK, 1989.

141. Sullivan, J.D. One pion exchange and deep inelastic electron—Nucleon scattering. *Phys. Rev. D* **1972**, *5*, 1732–1737. [CrossRef]

142. Bebek, C.J.; Brown, C.N. ; Holmes, S.D. ; Kline, R.V. ; Pipkin, F.M. ; Raither, S. ; Sisterson, L.K. ; Browman, A. ; Hanson, K.M. ; Larson, D.; et al. Electroproduction of single pions at low epsilon and a measurement of the pion form-factor up to $q^2 = 10$ GeV^2. *Phys. Rev. D* **1978**, *17*, 1693. [CrossRef]

143. Volmer, J.; Abbott, D. ; Anklin, H. ; Armstrong, C. ; Arrington, J. ; Assamagan, K. ; Avery, S. ; Baker, O.K. ; Blok, H.P. ; Bochna, C. ; Brash, E.J. ; et al. Measurement of the Charged Pion Electromagnetic Form-Factor. *Phys. Rev. Lett.* **2001**, *86*, 1713–1716. [CrossRef] [PubMed]

144. Huber, G.; Blok, H.P. ; Horn, T. ; Beise, E.J. ; Gaskell, D. ; Mack, D.J. ; Tadevosyan, V. ; Volmer, J. ; Abbott, D. ; Aniol, K. ; Anklin, H. ; Armstrong, C. ; Arrington, J. ; et al. Charged pion form-factor between Q**2 = 0.60-GeV**2 and 2.45-GeV**2. II. Determination of, and results for, the pion form-factor. *Phys. Rev.* **2008**, *C78*, 045203. [CrossRef]

145. Barry, P.C.; Sato, N.; Melnitchouk, W.; Ji, C.R. First Monte Carlo Global QCD Analysis of Pion Parton Distributions. *Phys. Rev. Lett.* **2018**, *121*, 152001. [CrossRef]

146. Barry, P.C.; Ji, C.R.; Sato, N.; Melnitchouk, W. Global QCD Analysis of Pion Parton Distributions with Threshold Resummation. *Phys. Rev. Lett.* **2021**, *127*, 232001. [CrossRef]
147. Amrath, D.; Diehl, M.; Lansberg, J.P. Deeply virtual Compton scattering on a virtual pion target. *Eur. Phys. J.* **2008**, *C58*, 179–192. [CrossRef]
148. Chávez, J.M.M.; Bertone, V.; De Soto Borrero, F.; Defurne, M.; Mezrag, C.; Moutarde, H.; Rodríguez-Quintero, J.; Segovia, J. Accessing the Pion 3D Structure at US and China Electron-Ion Colliders. *Phys. Rev. Lett.* **2022**, *128*, 202501. [CrossRef] [PubMed]
149. Belitsky, A.V.; Mueller, D. Refined analysis of photon leptoproduction off spinless target. *Phys. Rev.* **2009**, *D79*, 014017. [CrossRef]
150. Freund, A. On the extraction of skewed parton distributions from experiment. *Phys. Lett. B* **2000**, *472*, 412–419. [CrossRef]
151. Bertone, V.; Dutrieux, H.; Mezrag, C.; Moutarde, H.; Sznajder, P. The deconvolution problem of deeply virtual Compton scattering. *Phys. Rev. D* **2021**, *103*, 114019. [CrossRef]
152. Guidal, M.; Vanderhaeghen, M. Double deeply virtual Compton scattering off the nucleon. *Phys. Rev. Lett.* **2003**, *90*, 012001. [CrossRef] [PubMed]
153. Braun, V.M.; Ji, Y.; Schoenleber, J. Deeply Virtual Compton Scattering at Next-to-Next-to-Leading Order. *Phys. Rev. Lett.* **2022**, *129*, 172001. [CrossRef] [PubMed]
154. Novikov, I.; Abdolmaleki, H.; Britzger, D.; Cooper-Sarkar, A.; Giuli, F.; Glazov, A.; Kusina, A.; Luszczak, A.; Olness, F.; Starovoitov, P.; et al. Parton Distribution Functions of the Charged Pion Within The xFitter Framework. *Phys. Rev. D* **2020**, *102*, 014040. [CrossRef]
155. Gluck, M.; Reya, E.; Schienbein, I. Pionic parton distributions revisited. *Eur. Phys. J. C* **1999**, *10*, 313–317. [CrossRef]
156. Cornwall, J.M. Dynamical Mass Generation in Continuum QCD. *Phys. Rev. D* **1982**, *26*, 1453. [CrossRef]
157. Costa, C.S.R.; Freese, A.; Cloët, I.C.; El-Bennich, B.; Krein, G.a.; Tandy, P.C. Intrinsic glue and Wilson lines within dressed quarks. *Phys. Rev. C* **2021**, *104*, 045201. [CrossRef]
158. Ji, C.R.; Sill, A.F.; Lombard, R.M. Leading Order Perturbative QCD Calculation of Nucleon Dirac Form-factors. *Phys. Rev.* **1987**, *D36*, 165. [CrossRef] [PubMed]
159. Rodríguez-Quintero, J.; Binosi, D.; Mezrag, C.; Papavassiliou, J.; Roberts, C.D. Process-independent effective coupling. From QCD Green's functions to phenomenology. *Few Body Syst.* **2018**, *59*, 121. [CrossRef]
160. Hoodbhoy, P.; Ji, X.d.; Yuan, F. Probing quark distribution amplitudes through generalized parton distributions at large momentum transfer. *Phys. Rev. Lett.* **2004**, *92*, 012003. [CrossRef]
161. Riberdy, M.; Mezrag, C.; Segovia, J. Computing 3D nucleonic orbitals:an exploratory path with continuum QCD methods. 2023, *Under preparation*.
162. Segovia, J.; Cloet, I.C.; Roberts, C.D.; Schmidt, S.M. Nucleon and Δ elastic and transition form factors. *Few Body Syst.* **2014**, *55*, 1185–1222. [CrossRef]
163. Gutiérrez-Guerrero, L.X.; Paredes-Torres, G.; Bashir, A. Mesons and baryons: Parity partners. *Phys. Rev. D* **2021**, *104*, 094013 . [CrossRef]
164. Yin, P.L.; Cui, Z.F.; Roberts, C.D.; Segovia, J. Masses of positive- and negative-parity hadron ground-states, including those with heavy quarks. *Eur. Phys. J. C* **2021**, *81*, 327 . [CrossRef]
165. Eichmann, G.; Alkofer, R.; Krassnigg, A.; Nicmorus, D. Nucleon mass from a covariant three-quark Faddeev equation. *Phys. Rev. Lett.* **2010**, *104*, 201601. [CrossRef]
166. Eichmann, G.; Sanchis-Alepuz, H.; Williams, R.; Alkofer, R.; Fischer, C.S. Baryons as relativistic three-quark bound states. *Prog. Part. Nucl. Phys.* **2016**, *91*, 1–100. [CrossRef]
167. Wang, Q.W.; Qin, S.X.; Roberts, C.D.; Schmidt, S.M. Proton tensor charges from a Poincaré-covariant Faddeev equation. *Phys. Rev.* **2018**, *D98*, 054019. [CrossRef]
168. Ji, X.d.; Ma, J.P.; Yuan, F. Three quark light cone amplitudes of the proton and quark orbital motion dependent observables. *Nucl. Phys.* **2003**, *B652*, 383–404. [CrossRef]
169. Mezrag, C.; Segovia, J.; Chang, L.; Roberts, C.D. Parton distribution amplitudes: Revealing correlations within the proton and Roper. *Phys. Lett.* **2018**, *B783*, 263–267. [CrossRef]
170. Mezrag, C.; Segovia, J.; Ding, M.; Chang, L.; Roberts, C.D. Nucleon Parton Distribution Amplitude: A scalar diquark picture. In Proceedings of the 22nd International Conference on Few-Body Problems in Physics (FB22), Caen, France, 9–13 July 2018.
171. Barabanov, M.Y.; Bedolla, M.A.; Brooks, W.K.; Cates, G.D.; Chen, C.; Chen, Y.; Cisbani, E.; Ding, M.; Eichmann, G.; Ent, R.; et al. Diquark correlations in hadron physics: Origin, impact and evidence. *Prog. Part. Nucl. Phys.* **2021**, *116*, 103835. [CrossRef]
172. Radyushkin, A. Modeling Nucleon Generalized Parton Distributions. *Phys. Rev.* **2013**, *D87*, 096017. [CrossRef]
173. Anikin, I.V.; Teryaev, O.V. Dispersion relations and subtractions in hard exclusive processes. *Phys. Rev. D* **2007**, *76*, 056007. [CrossRef]
174. Diehl, M.; Ivanov, D.Y. Dispersion representations for hard exclusive processes: beyond the Born approximation. *Eur. Phys. J. C* **2007**, *52*, 919–932. [CrossRef]
175. Kumerički, K. Measurability of pressure inside the proton. *Nature* **2019**, *570*, E1–E2. [CrossRef]

176. Guichon, P.A.M.; Mossé, L.; Vanderhaeghen, M. Pion production in deeply virtual Compton scattering. *Phys. Rev. D* **2003**, *68*, 034018. [CrossRef]
177. Guidal, M.; Bouchigny, S.; Didelez, J.P.; Hadjidakis, C.; Hourany, E.; Vanderhaeghen, M. Generalized parton distributions and nucleon resonances. *Nucl. Phys. A* **2003**, *721*, 327–332. [CrossRef]